

1 **Semi-quantitative understanding of source contribution to nitrous**
2 **acid (HONO) based on 1-year continuous observation at the**
3 **SORPES station in eastern China**

4
5 Yuliang Liu^{1,2}, Wei Nie^{1,2*}, Zheng Xu^{1,2}, Tianyi Wang^{1,2}, Ruoxian Wang^{1,2},
6 Yuanyuan Li^{1,2}, Lei Wang^{1,2}, Xuguang Chi^{1,2}, and Aijun Ding^{1,2}

7
8 ¹Joint International Research Laboratory of Atmospheric and Earth System Sciences, School
9 of Atmospheric Sciences, Nanjing University, Nanjing, Jiangsu Province, China

10 ² Collaborative Innovation Center of Climate Change, Jiangsu Province, China

11
12 **Abstract**

13
14 Nitrous acid (HONO), an important precursor of the hydroxyl radical (OH), has been
15 long-standing recognized to be of significance to atmospheric chemistry, but its
16 sources are still debate. In this study, we conducted continuous measurement of
17 HONO from November 2017 to November 2018 at the SORPES station in Nanjing of
18 eastern China. The yearly average mixing ratio of observed HONO was 0.69 ± 0.58
19 ppb, showing a larger contribution to OH relative to ozone with a mean net OH
20 production rate of 0.67 ppb/h. To estimate the effect of combustion emissions of
21 HONO, the emitted ratios of HONO and NO_x were derived from 55 fresh plumes
22 (NO/NO_x > 0.85), with a mean value of 0.79%. During the nighttime, the chemistry of
23 HONO was found to depend on RH, and heterogeneous reaction of NO₂ on aerosol
24 surface was presumably responsible for HONO production. The average nighttime
25 NO₂-to-HONO conversion frequency (C_{HONO}) was determined to be 0.0055 ± 0.0032
26 h⁻¹ from 137 HONO formation cases. The missing source of HONO around noontime
27 seemed to be photo-induced with an average P_{unknown} of 1.04 ppb h⁻¹, based on a
28 semi-quantitative HONO budget analysis. An over-determined system of equations
29 was applied to obtain the monthly variations in nocturnal HONO sources. Except for
30 burning-emitted HONO (approximately 23% of total measured HONO), the
31 contribution of heterogeneous formation on ground surfaces was an approximately

32 constant proportion of 36% throughout the year. The soil emission revealed clear
33 seasonal variation, and contributed up to 40% of observed HONO in July and August.
34 A higher propensity for generating HONO on aerosol surface occurred in heavily
35 polluted period (about 40% of HONO in January). Our results highlight
36 ever-changing contributions of HONO sources, and encourage more long-term
37 observations to evaluate the contributions from varied sources.

38

39 **1. Introduction**

40

41 Nitrous acid (HONO) is a vital constituent of nitrogen cycle in the atmosphere, first
42 observed in the field by Perner and Platt (1979). The concentrations of HONO varied
43 from dozens of ppt in remote regions (Villena et al., 2011b;Meusel et al., 2016) to
44 several ppb in polluted urban regions (Yu et al., 2009;Tong et al., 2015). The
45 photolysis of HONO (R1) has been long standing as a momentous source of the
46 hydroxyl radicals (OH) especially during the early morning when other OH sources
47 are minor (Platt et al., 1980;Alicke, 2002, 2003). Even during the daytime, recent
48 studies have recognized the photolysis of HONO as a potentially stronger contributor
49 to daytime OH radicals than that of O₃ (Kleffmann, 2005;Elshorbany et al., 2009;Li et
50 al., 2018). Meanwhile, HONO has been found to affect adversely human health (Jarvis
51 et al., 2005;Sleiman et al., 2010).

52

53 Although the significance of HONO has been given much weight, the sources of
54 ambient HONO are complicated and have been debated for decades. HONO can be
55 emitted from combustion, including vehicle exhaust, industrial exhaust and biomass
56 burning (Table 1).Tunnel experiments with tests for different engine types have
57 determined an emission ratio of HONO/NO_x for traffic source, ranged in 0.3-0.8%
58 (Kirchstetter et al., 1996;Kurtenbach et al., 2001). The release from soil nitrite
59 through acidification reaction and partitioning is considered to be another primary
60 source of atmospheric HONO (Su et al., 2011). Soil nitrite could come from
61 biological nitrification and denitrification processes (Canfield et al., 2010;Oswald et
62 al., 2013), or be enriched via reactive uptake of HONO from the atmosphere

63 (VandenBoer et al., 2014a;VandenBoer et al., 2014b). In addition to direct emissions,
64 the vast majority of HONO is produced chemically. The recombination of NO and
65 OH (R3) is the main homogeneous reaction for supplying HONO (Pagsberg et al.,
66 1997;Atkinson, 2000), whose contribution may be significant under conditions of
67 sufficient reactants at daytime. During the nighttime, with low OH concentrations,
68 other larger sources, *i.e.* heterogeneous reactions of NO₂ on various surfaces, are
69 required to explain elevated mixing levels of HONO. Laboratory studies indicate that
70 NO₂ can be converted to HONO on humid surfaces (R4), being first order in NO₂ and
71 depending on various parameters including the gas phase NO₂ concentration, the
72 surface water content, and the surface area density (Kleffmann et al.,
73 1998;Finlayson-Pitts et al., 2003). Besides, *the* heterogeneous reduction of NO₂ with
74 surface organics (R5) is proposed to be another effective pathway to generate HONO
75 (Ammann et al., 1998;Ammann et al., 2005;Aubin and Abbatt, 2007), observed in
76 freshly emitted plumes with high concentrations of NO_x and BC (Xu et al., 2015).
77 Notably this reaction rate is drastically reduced after the first few seconds due to
78 consumption of the reactive surfaces (Kalberer et al., 1999;Kleffmann et al., 1999),
79 but this reaction could be strongly enhanced by light on photo-activated surface
80 (George et al., 2005;Stemmler et al., 2006;Stemmler et al., 2007). During the daytime,
81 heterogeneous HONO formation from the photolysis of adsorbed nitric acid (HNO₃)
82 and particulate nitrate (NO₃⁻) at UV wavelengths has been found in experiments and
83 observations (Zhou et al., 2003;Zhou et al., 2011;Ye et al., 2016;Ye et al., 2017).
84 Heterogeneous processes are typically considered as the primary sources of HONO in
85 many regions yet are the most poorly understood. For NO₂ conversion to HONO on
86 surfaces (R4,R5), the uptake coefficients of NO₂ derived from different experiments
87 vary from 10⁻⁹ to 10⁻² (Ammann et al., 1998;Kirchner et al., 2000;Underwood et al.,
88 2001;Aubin and Abbatt, 2007;Zhou et al., 2015). The key step to determine the
89 uptake of NO₂ or the reaction rate is still ill-defined, and we are also not certain if and
90 how the ambient natural surfaces can be reactivated by radiation. Furthermore, it has
91 become a main concern to compare the contributions of ground and aerosol surfaces
92 to HONO formation. It is so far, not well explained for the observed HONO,

93 especially during daytime. Large unknown sources of HONO were identified by many
94 studies (Su et al., 2008b;Sörgel et al., 2011;Michoud et al., 2014;Lee et al., 2016).

95
96 Benefitting from more and more studies, particularly the observations under different
97 environments (Lammel and Cape, 1996;Li et al., 2012), understanding of HONO
98 chemistry in the atmosphere has been greatly improved during the last decade.
99 However, most HONO observations were short-term campaigns with studies ranging
100 from several weeks to several months. For example, Reisinger (2000) found a linear
101 correlation between the HONO/NO₂ ratio and aerosol surface density in the polluted
102 winter atmosphere; and Nie et al. (2015) showed the influence of biomass burning
103 plumes on HONO chemistry, according to observed data during late April–June 2012;
104 while Wong et al. (2011) believed that NO₂ to HONO conversion on the ground was
105 the dominant source of HONO by analyzing vertical profiles from 15 August to 20
106 September in 2006. Moreover, a theory that HONO from soil emission explained the
107 strength and diurnal variations of the missing source has been presented by Su et al.
108 (2011) based on data measured from 23 to 30 October 2004. In case the HONO
109 sources possibly exhibit temporal variability, especially seasonal differences, it is
110 challenging to draw a full picture on the basis of these short-term observations. More
111 than a year of continuous observation is needed, yet rather limited.

112
113 The Yangtze River Delta (YRD) is one of the most developed regions in eastern
114 China. Rapid urbanization and industrialization have induced severe air pollution over
115 the last three decades, particularly high concentrations of reactive nitrogen (Richter et
116 al., 2005;Rohde and Muller, 2015), including HONO (Wang et al., 2013;Nie et al.,
117 2015). In this study, we [conducted HONO observations continuously from November
118 2017 to November 2018](#), at the Station for Observation Regional Processes and the
119 Earth System (SORPES), located in the western part of the YRD, a place that can be
120 influenced by air masses from different source regions of anthropogenic emissions,
121 biomass burning, dust and biogenic emissions (Ding et al., 2013;Ding et al., 2016).
122 Our one-year observation showed well-defined diurnal patterns and obvious season

123 variations of HONO concentrations at relatively high levels. We discussed the
124 potential mechanism of HONO production based upon semiquantitative analysis and
125 correlation studies, and paying special attention to changes in major sources of
126 HONO during different seasons.

127

128 **2. Methodology**

129

130 ***2.1. Study site and instrumentation***

131

132 Continuous observation was conducted at the SORPES station at the Xianlin Campus
133 of Nanjing University (118°57'E, 32°07'N), located in the northeast suburb of Nanjing,
134 China, from November 2017 to November 2018 (Fig. S1). The easterly prevailing
135 wind and synoptic condition makes it a representative background site of Nanjing and
136 a regional downwind site of the city cluster in the YRD region. Detailed descriptions
137 for the station can be found in previous studies (Ding et al., 2013;Ding et al., 2016).

138

139 HONO was measured with a commercial long path absorption photometer instrument
140 (QUAMA, Model LOPAP-03). The ambient air was sampled in two similar
141 temperature controlled stripping coils in series using a mixture reagent of 100 g
142 sulfanilamide and 1 L HCl (37% volume fraction) in 9 L pure water. In the first
143 stripping coil, all of the HONO and a fraction of interfering substances were absorbed
144 into solution, and the remaining interfering species (NO₂, HNO₃, HO₂NO₂, PAN, etc.)
145 were absorbed in the second stripping coil. After adding a reagent of 0.8 g
146 N-naphtylethylenediamine-dihydrochloride in 8 L pure water to, colored azo dyewas
147 formed in the solutions from 2 stripping coils, which were then separately detected via
148 long path absorption in special Teflon tubing. **To minimize the measurement**
149 **interferences**, the **real** HONO signal was the difference between the signals in the two
150 channels. Further details can be found in (Heland et al., 2001;Kleffmann et al., 2006).
151 To correct for the small drifts in instrument's baseline, **the** compressed air was
152 sampled every 12 h (flow rate: 1.0 L/min) to make zero measurement. A span check
153 was made using 0.04 mg/m³ nitrite (NO₂⁻) solution each two weeks with a flow rate of

154 0.28 ml/min. The time resolution, detection limit, accuracy of the measurement was 5
155 min, 10 pptv, and 10%, respectively.

156

157 The NO and NO₂ levels were measured using a chemiluminescence instrument (TEI,
158 model 42i) coupled with a highly selective photolytic converter (Droplet
159 Measurement Technologies, model BLC), and the analyzer had a detection limit of 50
160 pptv for an integration time of 5 min, with precision of 4% and an uncertainty of 10%
161 (Xu et al., 2013). Ozone and CO were measured continuously using Thermo-Fisher
162 Scientific TEI 49i and TEI 48i, *respectively*. The fine particle mass concentration
163 (PM_{2.5}) was continuously measured with a combined technique of light scattering
164 photometry and beta radiation attenuation (Thermo Scientific SHARP Monitor Model
165 5030). Water soluble aerosol ions (NO₃⁻, SO₄²⁻, NH₄⁺ etc.) and ammonia (NH₃) were
166 measured by a Monitor for Aerosols and Gases in ambient Air (designed and
167 manufactured by Applikon Analytical B.V., the Netherlands) with a PM_{2.5} cyclone
168 inlet, in a time resolution of 1 hr. The size distribution of submicron particles (6-820
169 nm) is measured with a DMPS (differential mobility particle sizer) constructed at the
170 University of Helsinki in Finland. Meteorological measurements including relative
171 humidity (RH), wind speed, wind direction, and air temperature were recorded by
172 Automatic Weather Station (CAMPEEL co., AG1000). UVB total radiation was
173 measured by UVB radiometer (UVS-B-T UV Radiometer, KIPP & ZONEN).

174

175 ***2.2. TUV model and OH estimate***

176

177 The Tropospheric Ultraviolet and Visible (TUV) Radiation Model
178 (<http://www.acd.ucar.edu/TUV>) was adopted to compute the photolysis frequencies,
179 which is most probably accurate in clean and cloudless days. The pivotal parameters
180 of this model were inputted as follows: the ozone density was measured by Total
181 Ozone Mapping Spectrometer (<http://toms.gsfc.nasa.gov/teacher/ozoneoverhead.html>);
182 the typical single scattering albedo (SSA) and Ångström exponent (Alpha) were 0.93
183 and 1.04 (Shen et al., 2018); The mean value of optical depth (AOD) at 550nm was
184 0.64, derived following an empirical relationship with PM_{2.5} in Nanjing (Shao et al.,

185 2017). To reduce the error of model, we used observed UVB to correct simulated
186 results (J_{mod}) by Eq. (1).

187

$$188 \quad J = \frac{\text{UVB}_{\text{obs}}}{\text{UVB}_{\text{mod}}} J_{\text{mod}} \quad (1)$$

189

190 The daytime OH concentration was calculated by applying the empirical model (Eq. 2)
191 proposed by Rohrer and Berresheim (2006), based on **strong** nearly linear correlations
192 of measured OH concentrations with simultaneously observed $J(\text{O}^1\text{D})$. **The coefficient**
193 **a** reflects the **average influence of reactants** (e.g. NO_x , VOCs, ozone, H_2O) **on OH** at
194 the selected place for research; the exponent **b** represents the combined effects of all
195 photolytic processes on OH, for example, $J(\text{O}^1\text{D})$, $J(\text{NO}_2)$, $J(\text{HONO})$, $J(\text{HCHO})$ and
196 **so on**; and the parameter **c** counts the light-independent OH sources. The values of
197 coefficients **a**, **b** and **c** in Eq. (2) are adopted from the OH studies in the Pearl River
198 Delta (PRD) and Beijing, China (Rohrer et al., 2014; Tan et al., 2017; Tan et al., 2018).
199 **By summarizing the coefficients a, b, c** in different OH observation campaigns (Table
200 **S1**), especially the almost equal slope of the OH- $J(\text{O}^1\text{D})$ relation for different
201 locations and seasons in the polluted areas of China, we can make assumptions that
202 the comprehensive impact of reactants (e.g. NO_x and VOCs) on OH cannot compete
203 with that of UV light to OH, and the chemical environments of OH are similar. This
204 suggest that it can be a reasonable way to derive OH by using Eq. (2) in our study,
205 and the error of derived OH radicals has been assessed as not subverting the relative
206 conclusions in this study (Fig. S1(a) and Fig. S1(d)). **The calculated OH**
207 **concentrations around noon** ($J(\text{O}^1\text{D}) > 1 \times 10^{-5} \text{ s}^{-1}$) were in the range of $0.46\text{-}2.0 \times 10^7$
208 cm^{-3} , comparable to observations in Chinese urban or suburban atmospheres (Lu et al.,
209 2012; Lu et al., 2013).

210

$$[\text{OH}] = a \times (\text{J}(\text{O}^1\text{D}) / 10^{-5} \text{s}^{-1})^b + c$$

$$a = 4.2 \times 10^6 \text{ cm}^{-3}, b = 1$$

211 $c = 1.0 \times 10^6 \text{ cm}^{-3}$ in summer (2)

$$c = 0.6 \times 10^6 \text{ cm}^{-3}$$
 in spring, autumn

$$c = 0.2 \times 10^6 \text{ cm}^{-3}$$
 in winter

212

213 **3. Results**

214

215 **3.1. Observation overview**

216

217 We carried out continuous measurements for HONO at the SORPES station in the
218 northeast suburb of Nanjing from November 2017 to November 2018 with a mean
219 measured ambient HONO mixing level of 0.69 ± 0.58 ppb (Fig. S2), within the range
220 of those in or in the vicinity of mega cities (Table 2). Fig.1 shows the seasonal pattern
221 of HONO and related parameters. The highest concentration of HONO was found in
222 winter (1.04 ± 0.75 ppb), followed by spring (0.68 ± 0.48 ppb), autumn (0.66 ± 0.53
223 ppb) and summer (0.45 ± 0.37 ppb). Such seasonal variations in Nanjing are aligned
224 with that in Beijing (Hendrick et al., 2014), and are somewhat similar to those in Jinan
225 (Li et al., 2018), where the highest levels occurred in winter and the lowest levels
226 occurred in autumn, but these variations are different from those in Hongkong (Xu et
227 al., 2015) where the highest and lowest values of HONO appeared in autumn and
228 spring, respectively. The important point is that the seasonality of HONO coincides
229 with that of NO_x (or NO_2), which is believed to be the main precursor of HONO in
230 current studies.

231

232 The HONO to NO_x ratio or the HONO to NO_2 ratio has been used extensively in
233 previous researches to characterize the HONO levels and to indicate the extent of
234 heterogeneous conversion of NO_2 to HONO, since it is less influenced by convection
235 or transport processes than the individual concentration (Lammel and Cape,
236 1996; Stutz et al., 2002). When a large proportion of HONO comes from direct
237 emissions, the value of HONO/NO_2 usually becomes larger, falsely implying the
238 strong formation of HONO from NO_2 . However, the freshly emitted air masses

239 generally have the lowest HONO/NO_x ratio, meaning that HONO/NO_x behaves better
240 than HONO/NO₂ in a way. As shown in Fig. 1(b), the low value of HONO/NO_x in
241 winter is attributed to heavy emissions because we see high mixing ratios of NO
242 during this cold season (Fig. 1c), the reasons for two peaks of HONO/NO_x in spring
243 and summer will be discussed in sections 3.3, 3.4 and 4.

244

245 All daily changes of HONO concentration in different seasons closely resemble a
246 cycle where HONO peaks in the early morning, and then decreases to the minimum in
247 the late afternoon, following the diurnal trend of NO_x (Fig. 2). The daily variations of
248 HONO in Nanjing are like those seen in other urban areas (Villena et al., 2011a; Wang
249 et al., 2013; Michoud et al., 2014; Lee et al., 2016), but differ from observations on the
250 roadside (Rappenglück et al., 2013; Xu et al., 2015). At night, the mixing ratio of
251 HONO increases rapidly in the first few hours and then stabilizes (in spring and
252 summer) or gradually climbs to its peak in the morning rush hour (in winter and
253 autumn). The accumulation during nighttime hours suggests a significant production
254 of HONO exceeding the dry deposition of HONO. As the sun rises, the HONO sink
255 will be strengthened by photolysis and the vertical mixing processes, resulting that the
256 peak times of the diurnal patterns of HONO concentration varies in different seasons.
257 During the daytime, the rate of HONO abatement is rapid before noon and then
258 becomes progressively until HONO concentration falling to the minimum. Given that
259 the photolytic lifetime of HONO is about 10-20 min at the midday (Stutz et al., 2000),
260 the considerable HONO concentration during daytime indicates the existence of
261 strong production of HONO.

262

263 From the daily variations of the HONO to NO_x ratio, we can further understand the
264 behavior of HONO in the atmosphere. the HONO/NO_x ratio is regularly enhanced
265 quickly before midnight then reaches a maximum during the latter half of the night.
266 According to Stutz et al. (2002), the highest HONO/NO_x (or HONO/NO₂) is defined
267 by the balance between production and loss of HONO at each night, the conditions
268 affecting the highest achievable ratio at nighttime will be discussed in section 3.3.

269 What's interesting here is the peak of the HONO/NO_x ratio in the midday sun in
 270 spring, summer and autumn, and even in winter, the ratio doesn't decline but remains
 271 stationary before and at noon. If the HONO sources during the daytime are consistent
 272 with those at night, the minimum HONO/NO_x ratio should occur at noon due to the
 273 intense photochemical loss of HONO. Therefore, there must be additional sources of
 274 HONO during daytime (e.g. R3). The increase of HONO/NO_x with solar radiation
 275 (e.g., UVB) is found in both diurnal and seasonal variations, indicating that these
 276 daytime sources have a relationship with the intensity of solar radiation. We will
 277 further discuss the potential daytime sources of HONO in section 3.4.

278

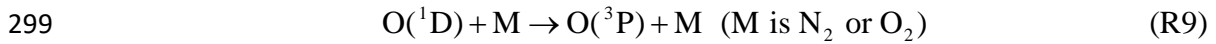
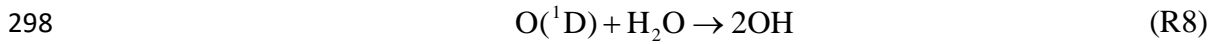
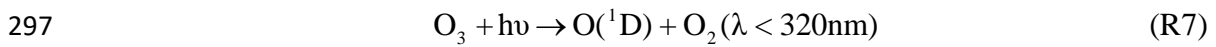
279 The elevated mixing ratio of HONO presents an efficient source of OH radicals
 280 during daytime in Nanjing. We calculate the net OH production rate from HONO, i.e.
 281 P_{OH}(HONO), using Eq. (3) (Li et al., 2018). For comparison, the OH production rate
 282 from ozone photolysis, P_{OH}(O₃), is derived from Eq. (4). Only part of the O(¹D) atoms,
 283 formed by the photolysis of O₃ at wavelengths below 320 nm (R7), can produce OH
 284 radicals by reacting with water (R8) in the atmosphere, so we use the absolute water
 285 concentration, which can be derived from relative humidity and temperature, to
 286 calculate the branching ratio of O(¹D)(φ_{OH}) between R8 and R9. The reaction rate of
 287 O(¹D) with O₂ is 4.0×10⁻¹¹ cm³ molecules⁻¹ s⁻¹ and the reaction rate of O(¹D) with N₂
 288 is 3.1×10⁻¹¹ cm³ molecules⁻¹ s⁻¹ (Seinfeld and Pandis, 2016). In addition to the two
 289 mechanisms mentioned above, there are other pathways to generate primary OH
 290 radicals: the photolysis of aldehydes, mainly HCHO, can form HO₂ radicals, and then
 291 converting to OH radicals by reacting with NO; the reactions of ozone with alkenes
 292 produce OH radicals directly (Finlayson-Pitts and Pitts, 2000; Seinfeld and Pandis,
 293 2016).

294

$$295 \quad P_{\text{OH}}(\text{HONO}) = J(\text{HONO})[\text{HONO}] - k_{\text{NO+OH}}[\text{NO}][\text{OH}] - k_{\text{HONO+OH}}[\text{HONO}][\text{OH}] \quad (3)$$

$$P_{OH}(O_3) = 2J(O^1D)[O_3]\phi_{OH} \quad (4)$$

$$\phi_{OH} = k_8[H_2O] / (k_8[H_2O] + k_9[M])$$



300

301 Fig. 3 shows that the diurnal peak of OH production rate from HONO is usually found
 302 in the late morning, caused by the combined effects of HONO concentration and its
 303 photolysis frequency, and the seasonal peak of $P_{OH}(HONO)$ occurs in spring for the
 304 same reason. $P_{OH}(O_3)$, coinciding with the trend of $J(O^1D)$, is highest around noon at
 305 daily time scale and is highest in summer at seasonal time scale, respectively.
 306 Significantly, the photolysis of HONO produce more OH than that of ozone
 307 throughout the daytime in winter, spring, and autumn. In summer, the contribution of
 308 HONO to OH is greater in the early morning, and although the photolysis of ozone
 309 contributes more OH at noon, the role of HONO is considerable. Overall, the average
 310 $P_{OH}(HONO)$ during 8:00-16:00 LT is 0.67 ppb/h, and the mean value of $P_{OH}(O_3)$ is
 311 0.41 ppb/h. The impressive role of HONO in the atmospheric oxidizing capacity
 312 should benefit photochemical ozone production (Ding et al., 2013; Xu et al., 2017; Xu
 313 et al., 2018), new particle formation (Qi et al., 2015) and secondary aerosol formation
 314 (Xie et al., 2015; Sun et al., 2018) in Nanjing, the western YRD region.

315

316 **3.2. Direct emissions of HONO from Combustion**

317

318 As mentioned above, the good correlation of HONO with NO_x (Fig. 4a) and the
 319 similar patterns of HONO and NO_x , particularly sharply increasing together in the
 320 fresh plumes, in which the NO/NO_x ratios are usually very high (Fig. S2), indicate the
 321 presence of direct combustion emission of HONO, which need to be deducted when
 322 analyzing the secondary formation of HONO. The SORPES station is influenced by
 323 air masses from both industries and vehicles (Ding et al., 2016), so the traffic
 324 emission factor investigated in other experiments cannot be used straightly. We derive

325 the emitted HONO/NO_x ratio according the method of Xu et al. (2015), and the
326 following criteria are adopted to select fresh plumes: (a) [NO_x] > 40 ppbv; (b)
327 $\Delta\text{NO}/\Delta\text{NO}_x > 0.85$; (c) good correlation between HONO and NO_x ($r > 0.9$); (d)
328 short duration of plumes (≤ 2 h); and (e) [UVB] ≤ 0.01 W/m². Then, the slopes of
329 HONO to NO_x in selected plumes were considered as the emission ratios in our study.

330

331 Within the one-year dataset, we select 55 freshly emitted plumes satisfying the criteria
332 above (Table S2), of which 20 air masses were found in the morning and evening rush
333 hours; the derived $\Delta\text{HONO}/\Delta\text{NO}_x$ ratios vary from 0.26% to 1.91% with a mean
334 value of $0.79\% \pm 0.36\%$. Many factors, such as the amount of excess oxygen; the types
335 of fuel used (gasoline, diesel, coal); if engines are catalyst-equipped, and if engines
336 are well-maintained, could result in variances in these ratios. Additionally, the rapid
337 heterogeneous reduction of NO₂ on synchronously emitted BC can also raise the value
338 of $\Delta\text{HONO}/\Delta\text{NO}_x$ (Xu et al., 2015). For our study, an average emission factor of
339 0.79% is deployed to evaluate the emission contribution of HONO (Eq. 5), which is
340 abbreviated as HONO_{emis}.

341

$$342 \quad \text{HONO}_{\text{emis}} = \text{NO}_x \times 0.0079 \quad (5)$$

$$343 \quad \text{HONO}_{\text{corr}} = \text{HONO} - \text{HONO}_{\text{emis}} \quad (6)$$

344

345 Combustion emissions contribute an average of 23% of total measured HONO
346 concentrations at night (Fig. 4b), with a maximum HONO_{emis}/HONO value of 32% in
347 winter and a minimum HONO_{emis}/HONO value of 18% in summer. We then get the
348 corrected observed HONO (HONO_{corr}) by Eq.(6) for further analysis. The slope of the
349 fitted line for HONO and NO_x is 1.62%, higher than emission ratio 0.79% (Fig. 4a),
350 and almost 80% of HONO is from HONO_{corr} that is not affected by emissions (Fig.
351 4b). These imply significant secondary formation of HONO in the atmosphere.

352

353 **3.3. Heterogeneous conversion of NO₂ to HONO during at nighttime**

354

355 **3.3.1. The NO₂-to-HONO conversion rate (C_{HONO})**

356

357 In addition to emissions, heterogeneous reaction of NO₂ on surfaces (R4, R5) is
358 believed to be the major formation pathways of nocturnal HONO. Thus, the
359 NO₂-to-HONO conversion rate is calculated from Eq. (5) (Alicke et al., 2002; Alicke,
360 2003; Wentzell et al., 2010), where NO₂ is adopted to scale HONO to reduce the
361 dilution influence according to Su et al. (2008a). Similar to HONO/NO_x (Fig. 2), the
362 nighttime HONO_{corr}/NO₂ ratio rises from the lowest value and then reaches a
363 quasi-stable state, meaning that C_{HONO} can actually be used to assess how quickly
364 HONO_{corr}/NO₂ can increase to its equilibrium.

365

$$366 \quad C_{\text{HONO}} = \frac{\frac{[\text{HONO}_{\text{corr}}]_{(t_2)}}{[\text{NO}_2]_{(t_2)}} - \frac{[\text{HONO}_{\text{corr}}]_{(t_1)}}{[\text{NO}_2]_{(t_1)}}}{t_2 - t_1} \quad (7)$$

367

368 Following the method of Xu et al. (2015) and Li et al. (2018), 137 cases in which
369 HONO_{corr}/NO₂ increased almost linearly from 18:00 to 24:00 each night are selected,
370 and the slope fitted by the least linear regression for HONO_{corr}/NO₂ against time is
371 just the conversion frequency of NO₂ to HONO. The derived C_{HONO} vary from
372 0.0043±0.0017 h⁻¹ in winter to 0.0066±0.0040 h⁻¹ in summer, with an average value
373 of 0.0055±0.0032 h⁻¹, which is in the range (0.004-0.014 h⁻¹) shown by other studies
374 in urban and suburban sites (Fig. 5). Noting that C_{HONO} assumes all the increase of
375 HONO_{corr}/NO₂ is caused by the conversion of NO₂, excluding other possible sources
376 of HONO (e.g. soil nitrite); and the computed C_{HONO} is the net NO₂-to-HONO
377 conversion rate since the measured HONO_{corr} has already taken the sinks of HONO
378 (mainly deposition) into account. Considering the uncertainties of C_{HONO}, utilizing
379 C_{HONO} directly to analyze the mechanism of HONO formation [thoroughly](#) may not be
380 appropriate, but it could be attemptable to facilitate the parameterizations for HONO
381 production in air quality models by C_{HONO} [when the chemical mechanisms are not](#)
382 [clear yet.](#)

383

384 **3.3.2. RH dependence of HONO chemistry**

385

386 It appears that NO_2 hydrolysis on humid surfaces (R4), having a first order
387 dependence on NO_2 (Jenkin et al., 1988; Ackermann, 2000; Finlayson-Pitts et al., 2003),
388 is influenced by the surface absorbed water (Kleffmann et al., 1998; Finlayson-Pitts et
389 al., 2003), although the exact mechanisms are still unknown. In the studies of Stutz et
390 al. (2002) and Stutz et al. (2004), the pseudo steady state of HONO/NO_2 , where this
391 ratio is at a maximum **at nighttime**, is presumed to be a balance between the
392 production of HONO from NO_2 and the loss of HONO on surfaces, and the highest
393 HONO/NO_2 value is determined by the ratio of the reactive uptake coefficients for
394 each process. Scatter plot of $\text{HONO}_{\text{corr}}/\text{NO}_2$ against relative humidity in our study are
395 illustrated in Fig. 6. **To eliminate as much influence of other factors as possible**, the
396 average of the 6 highest $\text{HONO}_{\text{corr}}/\text{NO}_2$ values in each 5% RH interval is calculated,
397 according to Stutz et al. (2004). The phenomenon that $\text{HONO}_{\text{corr}}/\text{NO}_2$ first increases
398 and then decreases with an increasing RH in Fig. 6(a) was also observed by other
399 studies (Hao et al., 2006; Yu et al., 2009; Li et al., 2012; Wang et al., 2013). The
400 dependencies of $\text{HONO}_{\text{corr}}/\text{NO}_2$ on RH and the possible reasons or mechanisms are
401 discussed as follows. **Even at the lowest measured RH of 18%, the absolute moisture
402 content in the atmosphere is still greater than 10^3 ppm in our study, which is quite
403 abundant to react with NO_2 , but the $\text{HONO}_{\text{corr}}/\text{NO}_2$ ratio is quite small and remains
404 unchanged when RH is below 45%, indicating that the NO_2 to HONO conversion
405 efficiency should be determined by water covering the surfaces, rather than by the
406 amount of water in the air.**

407

408 It has been reported that surfaced absorbed water depends on RH values, and the
409 dependences vary for different material surfaces of the ground, but generally follow
410 the shape of a BET isotherm (Lammel, 1999; Saliba et al., 2001; Sumner et al., 2004).
411 The number of mono-layers of water increases slowly from zero to 2-4, accompanied
412 by RH from zero to a turning point, and the water coverage grows dramatically (up to
413 10-100 mono-layers) once RH exceeds the turning point (Finlayson-Pitts et al., 2003).
414 Fig. 6(a) shows the case where the surface for NO_2 converting to HONO is dominated
415 by the ground, the $\text{HONO}_{\text{corr}}/\text{NO}_2$ increases along with RH when RH is less than 75%,

416 which can be explained by the reaction of NO_2 to generate HONO on wet surfaces.
417 However, a negative correlation between $\text{HONO}_{\text{corr}}/\text{NO}_2$ and RH is found when RH is
418 over 75%, presumably because that the rapidly growing aqueous layers of the ground
419 surface lead to efficient uptake of HONO and make the surface less accessible or less
420 reactive for NO_2 . Hence, the RH turning point for absorbed water on ground surfaces
421 is perhaps around 75% for our observation, within the range of results from
422 experiments on various surfaces (70-80% RH) (Lammel, 1999; Saliba et al.,
423 2001; Sumner et al., 2004). Once RH exceeds 95%, the reaction surface is
424 asymptotically approaching the state of water droplet, where the quite limited
425 formation of HONO and the extremely impactful loss of HONO will result in a
426 dramatic decline of the $\text{HONO}_{\text{corr}}/\text{NO}_2$ ratio (Fig. 6(a) and Fig. 6(b)).

427

428 Notably, the constant $\text{HONO}_{\text{corr}}/\text{NO}_2$ value at RH between 75-95% under the
429 condition of high $\text{PM}_{2.5}$ mass loading (Fig. 6(b)), compared to the downward trend of
430 $\text{HONO}_{\text{corr}}/\text{NO}_2$ within the same humidity range in low $\text{PM}_{2.5}$ mass concentration (Fig.
431 6(a)), implies a contribution of aerosol surfaces to the NO_2 -HONO conversion. Since
432 both $\text{HONO}_{\text{corr}}/\text{NO}_2$ in Fig. 6(a) and Fig. 6(b) are affected by the ground surfaces, we
433 can use the difference of $\text{HONO}_{\text{corr}}/\text{NO}_2$ between the two figures to represent the
434 influence of aerosol. As the area of shadow showed in Fig. 6(b), the aerosol-affected
435 $\text{HONO}_{\text{corr}}/\text{NO}_2$ is positively related to RH before RH reaches 95%. With the increase
436 of RH, the hygroscopic growth of aerosol particles should provide larger surface area.
437 When RH is higher than 75%, which has exceeded the mutual deliquescence relative
438 humidity of inorganic salts (Fountoukis and Nenes, 2007), aerosols will transfer to
439 aqueous phase gradually, and then promoting multiphase or heterogeneous chemistry
440 processes (Herrmann et al., 2015). For example, the oxidation of SO_2 by NO_2 on
441 aqueous aerosol surface may produce $\text{NO}_2^-/\text{HONO}$ efficiently under polluted
442 condition (Xie et al., 2015; Wang et al., 2016). In addition, the enhancement NO_2
443 uptake on micro-droplets by anions has been reported in experiments (Yabushita et al.,
444 2009)

445

446 3.3.3. Impact of aerosols on HONO formation

447

448 To further understand the heterogeneous formation of HONO on aerosol, we carry out
449 a correlation analysis when $\text{HONO}_{\text{corr}}/\text{NO}_2$ reaches the pseudo steady state at each
450 night (3:00-6:00 LT). The convergence or diffusion processes of gases and particles
451 caused by the decrease or increase of the boundary layer height can also lead to a
452 consistent trend of $\text{HONO}_{\text{corr}}$ and $\text{PM}_{2.5}$ (Fig. 7a), while the ratio of $\text{HONO}_{\text{corr}}$ and
453 NO_2 can not only reduce this physical effect but also represent the conversion degree
454 of NO_2 to HONO, so a moderate positive correlation between $\text{HONO}_{\text{corr}}/\text{NO}_2$ and
455 $\text{PM}_{2.5}$ ($r=0.35$, $p=0.01$) throughout the observation period could be more convincing
456 (Fig. 7b). As shown by larger triangles with gray borders in Fig. 7(b), $\text{HONO}_{\text{corr}}/\text{NO}_2$
457 is better correlated with $\text{PM}_{2.5}$ in the months when the mass concentrations of $\text{PM}_{2.5}$
458 are higher during this 1-year measurement, generally occurring from November to
459 May (Fig. 1d). This finding can be explained with a law that greater contributions of
460 NO_2 heterogeneously reacting on aerosol surface to HONO cause better correlations
461 between $\text{HONO}_{\text{corr}}/\text{NO}_2$ and $\text{PM}_{2.5}$. Interestingly, this relationship can also be divided
462 approximately into two groups by NH_3/CO ; the correlation is good when the value of
463 NH_3/CO is lower than 2‰, but when NH_3/CO is higher than 2‰, a poor correlation is
464 found. We will discuss this phenomenon further in section 4. The evidence of HONO
465 formation on aerosol were also found in other observations (Reisinger, 2000; Wang,
466 2003; Li et al., 2012; Nie et al., 2015; Hou et al., 2016; Cui et al., 2018).

467

468 As is known, producing HONO is not the dominant sink of NO_2 at night, but it seems
469 that more NO_2 can be converted to HONO under conditions of heavy pollution (Fig.
470 7b). We discuss whether heterogeneous reactions of NO_2 on aerosols are able to
471 provide comparable HONO with our measurement by Eq. (8), only considering
472 HONO formation on particle surfaces and assuming that HONO principally settles on
473 the ground surface, neglecting HONO loss on aerosol. c_{NO_2} is the mean molecular

474 velocity of NO_2 (370m/s); $[\frac{S}{V}]_{\text{aer}}$ is the surface area to volume ratio (m^{-1}) of aerosol;

475 v_{HONO} is the deposition velocity of HONO, which is considered to be close to the
 476 deposition velocity of NO_2 at night (Stutz et al., 2002; Su et al., 2008a); and a
 477 approximate value of 0.1 cm/s is used based on the measurements from Coe and
 478 Gallagher (1992) and Stutz et al. (2002); H is the boundary layer mixing depth, and a
 479 value of 100 m is assumed for nighttime (Su et al., 2008a).

480

$$481 \quad C_{\text{HONO}} = \frac{1}{4} \gamma_{\text{NO}_2 \rightarrow \text{HONO}} c_{\text{NO}_2} \left[\frac{S}{V} \right]_{\text{aer}} - \frac{v_{\text{HONO}} [\text{HONO}]}{H [\text{NO}_2]} \quad (8)$$

482

483 Considering at nighttime period with severe haze, the aerosol surface density
 484 calculated from the particle number size distributions between 6 nm and 800 nm is
 485 about $1.2 \times 10^{-3} \text{ m}^{-1}$, matched by $200 \mu\text{g}/\text{m}^3$ of $\text{PM}_{2.5}$ from our observations, and the
 486 averaged mixing ratios of HONO and NO_2 are 1.15 ppb and 28.4 ppb, respectively
 487 (Table 2). For 30%-100% of the measured mean C_{HONO} (0.0043 h^{-1}) in winter, the
 488 uptake coefficient of NO_2 -to-HONO ($\gamma_{\text{NO}_2 \rightarrow \text{HONO}}$) calculated from Eq. (8) is in the range

489 of 6.9×10^{-6} to 1.44×10^{-5} , consistent with the results from many laboratory studies

490 which demonstrate that the uptake coefficients of NO_2 (γ_{NO_2}) on multiple aerosol

491 surfaces or wet surfaces are mainly distributed around 10^{-5} with the HONO yield

492 varying from 0.1 to 0.9 (Grassian, 2002; Aubin and Abbatt, 2007; Khalizov et al.,

493 2010; Han et al., 2017). It is necessary to elaborate that: (1) the ambient particles were

494 dried with silica gel before measuring their number size distributions, and the mass

495 concentrations of $\text{PM}_{2.5}$ were also measured under a system where the temperature

496 was maintained at 30°C , usually above ambient temperature; (2) the aerosol surface

497 was calculated by assuming that all particles are spherically shaped, but the particles

498 could in fact have irregular bodies and porous structure; (3) the particle size of both

499 $\text{PM}_{2.5}$ and derived $\left[\frac{S}{V} \right]_{\text{aer}}$ is just a part of the total suspended particulate matter. As

500 described, the aerosol surface in the atmosphere is actually underestimated in our

501 study, thus the $\gamma_{\text{NO}_2 \rightarrow \text{HONO}}$ we derived could be the upper limit of the uptake coefficient

502 for NO₂ conversion to HONO on aerosol. In addition to particles surfaces, other
 503 aerosol parameters such as surface water content, chemical composition, pH value,
 504 and phase state of surfaces may also influence the heterogeneous formation of
 505 HONO.

506

507 **3.4. Missing daytime HONO source**

508

509 After discussing the nocturnal formation mechanism of HONO, we now focus on
 510 the chemistry of daytime HONO whose concentrations are still about 0.25-0.6 ppb at
 511 noon with a lifetime of only 10-20 min (Fig. 2). We are not certain if the observed
 512 HONO can be provided by known mechanisms (gas phase reaction (R4) and
 513 emissions) to date, so a budget equation of daytime HONO (Eq. 9) is utilized to
 514 analyze its source and sinks (Su et al., 2008b;Sörgel et al., 2011). Here, dHONO/dt is
 515 the change rate of the observed HONO. The sources rates of HONO contain the
 516 homogeneous formation rate (P_{NO+OH}, R3); the combustion emission rate (P_{emis}); and
 517 the unknown HONO daytime source (P_{unknown}). The sink rates of HONO consist of the
 518 photolysis rate (L_{phot}, R1); the reaction rate of HONO with OH (L_{HONO+OH}, R2); and
 519 the dry deposition rate (L_{dep}). T_v and T_h represent the vertical (T_v) and horizontal (T_h)
 520 transport processes of HONO, which are thought to be negligible for intense radiation
 521 and relatively homogeneous atmospheres with generally calm winds (Dillon, 2002;Su
 522 et al., 2008b;Sörgel et al., 2011).

523

$$524 \quad \frac{dHONO}{dt} = (P_{NO+OH} + P_{emis} + P_{unknown}) - (L_{phot} + L_{HONO+OH} + L_{dep}) + T_v + T_h \quad (9)$$

525

526 Therefore, the undiscovered daytime source of HONO (P_{unknown}) can be derived by Eq.
 527 (10), which is a deformation of Eq. (9) without minor terms (T_v and T_h) and where
 528 dHONO/dt is substituted by ΔHONO/Δt that is counted as difference between
 529 observed HONO at two time points. The reaction rate constants of reaction 2
 530 (k_{HONO+OH}) and reaction 3 (k_{NO+OH}) are 6.0×10⁻¹² cm³ molecules⁻¹ s⁻¹ and 9.8×10⁻¹²
 531 cm³ molecules⁻¹ s⁻¹, respectively (Atkinson et al., 2004). The emission ratio of

532 HONO and NO_x (HONO/NO_x=0.79%) obtained in section 3.2, is used to estimate
 533 P_{emis}. For L_{dep}, the dry deposition velocity of diurnal HONO (v_{HONO}) is measured as
 534 2cm/s in the work of Harrison et al. (1996), and a practical mixing height of 200m is
 535 adopted, considering that most of the HONO cannot rise above this altitude due to
 536 rapid photolysis (Alicke et al., 2002). **It is worthy of mention that although we did not**
 537 **observe OH radicals directly, the uncertainty of P_{unknown} caused by the calculated OH**
 538 **radicals from Eq. (2) can be reduced substantially in the case of low concentration of**
 539 **NO and high value of J(O¹D) (Fig. S1(d)).**

540

$$541 \quad P_{\text{unknown}} = J(\text{HONO})[\text{HONO}] + k_{\text{HONO+OH}}[\text{HONO}][\text{OH}] + \frac{v_{\text{HONO}}}{H}[\text{HONO}] \quad (10)$$

$$+ \frac{\Delta \text{HONO}}{\Delta t} - k_{\text{NO+OH}}[\text{NO}][\text{OH}] - \frac{0.79\% \times \Delta \text{NO}_x}{\Delta t}$$

542

543 Fig. 8 shows the average daytime HONO budget from 8:00 LT to 16:00 LT during
 544 different seasons. The major loss route of HONO is photodecomposition (L_{phot}) with
 545 an average value of 1.50 ppb/h around noontime (10:00-14:00 LT) during this
 546 observation period, next to dry deposition (L_{dep}) whose mean value at the same time is
 547 0.21 ppb/h, and by L_{HONO+OH} which is less than 5% of that of L_{phot}. For the sources of
 548 HONO around noon, the average homogeneous reaction rate between NO and OH
 549 (P_{NO+OH}) is 0.63 ppb/h and P_{emis} just gives a tiny part of HONO at a rate of 0.02 ppb/h,
 550 meaning that most of HONO comes from an unknown source whose average rate
 551 (P_{unknown}) is 1.04 ppb/h, contributing about 61% of the production of HONO.
 552 Comparing summer data, the mean unknown daytime source strength of HONO in
 553 Nanjing is almost at the upper-middle level of those reported in the existing literature:
 554 0.22 ppb/h at a rural site of New York state, USA (Zhou et al., 2002); 0.5 ppb/h in a
 555 forest near Jülich, Germany (Kleffmann, 2005); 0.77 ppb/h in a polluted rural area of
 556 the Pearl River Delta, China (Li et al., 2012); 0.98 ppb/h at an urban site in Xi'an,
 557 China (Huang et al., 2017); 1.7 ppb/h in an urban area of Santiago, Chile (Elshorbany
 558 et al., 2009); 2.95 ppb/h in the urban atmosphere of Jinan, China (Li et al., 2018). **In**
 559 **our study, the OH production rate from the missing HONO accounts for about 76% of**

560 total $P_{OH}(HONO)$ (Fig. S2), suggesting that the unconventional source of HONO is of
561 significance to atmospheric oxidation.

562

563 Hence, we perform a correlation analysis to explore the potential unknown daytime
564 mechanisms of HONO (Table 3). $P_{unknown}$ is better correlated with NO_2*UVB than
565 with NO_2 or UVB alone in winter, spring and autumn ($p=0.05$), perhaps associated
566 with the photo-enhanced conversion from NO_2 to HONO (George et al.,
567 2005;Stemmler et al., 2006;Stemmler et al., 2007). The average value of $P_{unknown}$
568 normalized by NO_2 is $0.1 h^{-1}$, over 18 times greater than the nighttime conversion rate
569 ($0.0055 h^{-1}$), also implying that $P_{unknown}$ cannot be explained by the nocturnal
570 mechanism of NO_2 -to-HONO. Assuming that the height of a well-mixed boundary
571 layer around noon remains constant for each day, $UVB*NO_2$ and $UVB*NO_2*PM_{2.5}$
572 could be proxies for photo-induced heterogeneous reactions of NO_2 on ground and
573 aerosol surfaces, respectively. We do not have any solid evidence to identify which
574 surfaces (ground or aerosol) are more important to the photo-heterogeneous reaction
575 of NO_2 based on the present analysis. For the same reason, the photolysis of
576 particulate nitrates (NO_3^-) as a source of HONO (Ye et al., 2016;Ye et al., 2017)
577 cannot be determined whether it is momentous in our study. The comparisons of
578 correlation coefficients showed above follow the method provided by Meng et al.
579 (1992).

580

581 Our study suggest that the missing source of HONO should be considered in the air
582 quality forecasting or regional models to characterize atmospheric oxidizing capacity
583 better, especially in warm seasons (spring and summer). Based on the measurement
584 (Fig. S3), the light-induced heterogeneous conversion of NO_2 to HONO on aerosol
585 surfaces and ground surface can been included in simulation works probably, as what
586 did in Lee et al. (2016).

587

588 *4. Semi-quantitative estimation of the contribution from different sources*

589

590 From this and previous studies, we can conclude that not only the concentration of

591 ambient HONO but also the sources of HONO have temporal and spatial patterns,
592 which is supposed to be considered in model studies. Nocturnal HONO is selected to
593 discuss the monthly variations of HONO sources in detail without the uncertainties of
594 daytime HONO formation, the influences of HONO photolysis, and the mixing effect
595 of boundary layer. The heterogeneous reaction of NO₂ on aerosol produces a
596 considerable portion of HONO in relatively polluted months (Dec.-May), but
597 contributes very little less than nothing in clean months (Jun.-Oct.), as seen in section
598 3.3.3. Coincidentally, direct emissions from burning processes of HONO decrease
599 from their peak values from winter to summer (section 3.2). However, the monthly
600 averaged ratios of HONO and NO_x are highest in summer, which conflicts with the
601 two sources mentioned above.

602

603 As is known, higher NO₂-to-HONO conversion level or other NO_x-independent
604 sources can cause an increase in the HONO/NO_x ratio. For the case of a mostly
605 constant surface with low reactivity due to the prolong exposure to oxidizing gases
606 and radiation, the yield of nighttime HONO from NO₂ reacting on ground surfaces
607 could be imprecisely assumed to be unchanged. Thus, soil nitrite formed through
608 microbial activities, especially nitrification by ammonia-oxidizing bacteria
609 (NH₄⁺→NO₂⁻) (Su et al., 2011;Oswald et al., 2013), is adopted to be an source for
610 atmospheric HONO in this study, considering the nearby presence of some grassland
611 and natural vegetation mosaics. Although we do not directly measure HONO
612 emissions from soil, the observed ammonia can represent its monthly average
613 intensity indirectly, based on the following hypothesis: the dominant source of NH₃ is
614 from soil, especially from fertilizers (NH₄⁺→NH₃) for a good correlation between
615 ammonia and temperature in the site (r=0.63, p=0.01), omitting the contributions of
616 livestock to NH₃ since there is only a small poultry facility within 10 km of this site
617 (Meng et al., 2011;Huang et al., 2012;Behera et al., 2013). Combustion sources
618 (vehicles, industry, biomass burning) should contribute only a fraction of NH₃ seeing
619 that NH₃ is not related to NO_x or CO in our study. Moreover, the release of both
620 HONO and NH₃ depend on the strength of microbial activities, fertilizing amount, and

621 soil properties (e.g., temperature, acidity and water content of soil). Although the
622 processes of HONO and NH₃ emission from soil may not be completely synchronized,
623 the seasonal patterns for each should be consistent.

624

625 Until now, we can separate the sources of HONO into four parts: (1) the combustion
626 emissions from vehicles and industries (HONO_{emi}) with a constant emitted
627 HONO/NO_x ratio of 0.79%; (2) the conversion of NO₂ to HONO on the ground
628 surfaces (HONO_{grd}) with a constant but unknown yield x_1 ; (3) the conversion of NO₂
629 to HONO on aerosol surfaces (HONO_{aer}) with a PM_{2.5}-dependent yield
630 (HONO_{aer}/NO₂); and (4) emission from soil (HONO_{soi}), expressed by corrected NH₃
631 multiplied by an unknown coefficient x_2 . The corrected NH₃ is obtained by
632 subtracting combustion emission from total observed ammonia. Ammonia from
633 combustion is found to be proportional to simultaneous CO (Meng et al., 2011; Chang
634 et al., 2016), and a proportion of 0.3%, which is in the lower quantile of the
635 NH₃/CO ratios in fresh air masses (for hourly data: NO/NO_x>0.75; UVB=0;
636 temperature<5°C) is used from our measurements. Substituting monthly average
637 values of measured HONO, NO₂, PM_{2.5}, NH₃, and CO into Eq.(11) by assuming that
638 HONO_{tot} is equal to HONO_{obs}, we can get an overdetermined system of equations,
639 which have 11 equations with 2 unknowns (excluding mean values of related
640 parameters from February), and then we derive an approximate solution ($x_1=1.89%$,
641 $x_2=1.62%$) by the method of ordinary least squares.

642

643 Fig. 9 shows that an average of 36% of HONO is produced heterogeneously on
644 ground surfaces without perceptible temporal variations, but the contribution of this
645 source is overtaken by NO₂ converting to HONO on aerosols in January
646 (approximately 40% of HONO), and was exceeded by soil emission in July and
647 August (approximately 40% of HONO). The seasonal variations of HONO from
648 different pathways at night indicate that short-term observations may just capture a
649 small part of the total picture when exploring the source mechanisms of HONO. The
650 total HONO concentration (HONO_{tot}) is the sum of derived HONO from the four

651 sources listed above. The good correlation between HONO_{tot} and HONO_{obs} and the
652 low mean normalized error of HONO_{tot} to HONO_{obs} reveal that our assumption on
653 nocturnal HONO sources is reasonable. It should be noted that the slope of the
654 linearly fitted line between HONO_{corr}/NO₂ and PM_{2.5} in spring (r=0.74, slope=0.68‰)
655 is much higher than that in winter (r=0.60, slope=0.20‰), but we just use a mean
656 slope of 0.26‰ to evaluate aerosol effects throughout the year, this may be why our
657 method underestimates HONO in March and April and overestimates HONO in
658 January, and indicating that the mass concentration of PM_{2.5} is not the only factor
659 affecting formation of HONO on aerosols. Besides, lacking considerations of the
660 impact of RH and temperature on NO₂-to-HONO conversion and of seasonal
661 variations in ground surface properties, uncertainties of NO₂-to-HONO conversion
662 mechanisms and of combustion HONO emissions, and lacking direct observation for
663 soil emitted HONO, could all result in the bias between HONO_{tot} and HONO_{obs}, so
664 more studies on the detailed mechanism of various HONO sources need to be
665 performed.

666

$$\begin{aligned}
\frac{[\text{HONO}_{\text{grd}}]}{[\text{NO}_2]} &= x_1 \\
\frac{[\text{HONO}_{\text{aer}}]}{[\text{NO}_2]} &= 0.26\% \times [\text{PM}_{2.5}] \\
\frac{[\text{HONO}_{\text{emi}}]}{[\text{NO}_x]} &= 0.79\% \tag{11} \\
\frac{[\text{HONO}_{\text{soi}}]}{[\text{NH}_3] - 0.3\% \times [\text{CO}]} &= x_2 \\
[\text{HONO}_{\text{tot}}] &= [\text{HONO}_{\text{emi}}] + [\text{HONO}_{\text{soi}}] + [\text{HONO}_{\text{grd}}] + [\text{HONO}_{\text{aer}}]
\end{aligned}$$

668

669 *5. Conclusions*

670

671 Continuous field measurement of HONO over 1 year was conducted at the SORPES
672 station in Nanjing in the western YRD of China, from December 2017 to
673 December 2018. The observed seasonal average concentrations of HONO are in the
674 range of 0.45-1.04 ppb, which are comparable to those in other urban or suburban
675 regions and appears to be of vital importance to atmospheric oxidation as the net OH

676 production rate of HONO is **over 1.5** times as that of ozone at daytime. HONO and
677 NO_x have coincident monthly variations peaking in December and decreasing to the
678 lowest value in August, and have similar diurnal pattern with the highest value in the
679 early morning and a low point in the late afternoon, both indicating that NO_x is a
680 crucial precursor of HONO.

681

682 Combustion emissions contribute an average of 23% to nocturnal HONO
683 concentrations, with an average emission ratio $\Delta\text{HONO}/\Delta\text{NO}_x$ of 0.79%. During the
684 nighttime, the dominant source of RH-dependent HONO could be the heterogeneous
685 reaction of NO₂ on wet ground or aerosol surfaces with a mean estimated conversion
686 rate of 0.0055 h⁻¹. During the daytime, a missing HONO source with an average
687 strength of **1.04** ppb/h was identified around noon, contributing about **61%** of the
688 production of HONO and seeming to be photo-enhanced. HONO released from soil is
689 adopted to discuss the seasonal changes of nocturnal HONO, and can contribute 40%
690 to HONO during summer. Ground formation provides a major part of HONO at a
691 roughly constant proportion of 36%. The uptake of NO₂ on aerosol surface could
692 generate the greatest amount of HONO during heavily polluted periods (e.g. January).
693 Our results draw a complete picture of the sources of HONO during different seasons,
694 and demonstrated the needs of long-term and comprehensive observations to improve
695 the understanding of HONO chemistry.

696 **Author contribution**

697 W.N. and A.D. designed the study; Y.L. and W.N. wrote the manuscript; Y.L., Z.X.
698 and R.X. collected the HONO data and contributed to the data analysis; T.W., Y.L.,
699 L.W. and X.C. collected other related data, e.g. NH₃, NO_x and PM_{2.5}.

700 **Acknowledgments**

701 This work was mainly funded by the National Key R&D Program of China
702 (2016YFC0202000 and 2016YFC0200500), the National Natural Science Foundation
703 of China (NSFC) project (D0512/41675145 and D0510/41605098), and Jiangsu

704 Provincial Science Fund (BK20160620). Data analysis was also supported by other
705 NSFC projects (D0512/41875175 and D0510/41605098).

706 **References**

707

708 Acker, K., Febo, A., Trick, S., Perrino, C., Bruno, P., Wiesen, P., Möller, D., Wieprecht, W.,
709 Auel, R., and Giusto, M.: Nitrous acid in the urban area of Rome, *Atmos. Environ.*, 40,
710 3123-3133, 2006.

711 Ackermann, R.: Auswirkungen von Kraftfahrzeugemissionen in der urbanen Atmosphäre,
712 Dissertation. de, 2000.

713 Alicke, B.: Impact of nitrous acid photolysis on the total hydroxyl radical budget during the
714 Limitation of Oxidant Production/Pianura Padana Produzione di Ozono study in Milan,
715 *Journal of Geophysical Research*, 107, 10.1029/2000jd000075, 2002.

716 Alicke, B., Platt, U., and Stutz, J.: Impact of nitrous acid photolysis on the total hydroxyl
717 radical budget during the Limitation of Oxidant Production/Pianura Padana Produzione di
718 Ozono study in Milan, *Journal of Geophysical Research: Atmospheres*, 107, LOP 9-1-LOP
719 9-17, 2002.

720 Alicke, B.: OH formation by HONO photolysis during the BERLIOZ experiment, *Journal of*
721 *Geophysical Research*, 108, 10.1029/2001jd000579, 2003.

722 Ammann, M., Kalberer, M., Jost, D., Tobler, L., Rossler, E., Piguet, D., Gaggeler, H., and
723 Baltensperger, U.: Heterogeneous production of nitrous acid on soot in polluted airmasses,
724 *NATURE*, 395, 157-160, 10.1038/25965, 1998.

725 Ammann, M., Rossler, E., Strekowski, R., and George, C.: Nitrogen dioxide multiphase
726 chemistry: uptake kinetics on aqueous solutions containing phenolic compounds, *Phys Chem*
727 *Chem Phys*, 7, 2513-2518, 10.1039/b501808k, 2005.

728 Atkinson, R.: Atmospheric chemistry of VOCs and NO_x, *Atmos. Environ.*, 34, 2063-2101,
729 2000.

730 Atkinson, R., Baulch, D., Cox, R., Crowley, J., Hampson, R., Hynes, R., Jenkin, M., Rossi,
731 M., and Troe, J.: Evaluated kinetic and photochemical data for atmospheric chemistry:
732 Volume I-gas phase reactions of O_x, HO_x, NO_x and SO_x species, *Atmospheric chemistry*
733 *and physics*, 4, 1461-1738, 2004.

734 Aubin, D. G., and Abbatt, J. P.: Interaction of NO₂ with hydrocarbon soot: Focus on HONO
735 yield, surface modification, and mechanism, *The Journal of Physical Chemistry A*, 111,
736 6263-6273, 2007.

737 Behera, S. N., Sharma, M., Aneja, V. P., and Balasubramanian, R.: Ammonia in the
738 atmosphere: a review on emission sources, atmospheric chemistry and deposition on
739 terrestrial bodies, *Environ Sci Pollut Res Int*, 20, 8092-8131, 10.1007/s11356-013-2051-9,
740 2013.

741 Bernard, F., Cazaunau, M., Grosselin, B., Zhou, B., Zheng, J., Liang, P., Zhang, Y., Ye, X.,
742 Daele, V., Mu, Y., Zhang, R., Chen, J., and Mellouki, A.: Measurements of nitrous acid
743 (HONO) in urban area of Shanghai, China, *Environ Sci Pollut Res Int*, 23, 5818-5829,
744 10.1007/s11356-015-5797-4, 2016.

745 Canfield, D. E., Glazer, A. N., and Falkowski, P. G.: The Evolution and Future of Earth's
746 Nitrogen Cycle, *Science*, 330, 192-196, 10.1126/science.1186120, 2010.

747 Chang, Y., Zou, Z., Deng, C., Huang, K., Collett, J. L., Lin, J., and Zhuang, G.: The
748 importance of vehicle emissions as a source of atmospheric ammonia in the megacity of
749 Shanghai, *Atmospheric Chemistry and Physics*, 16, 3577, 2016.

750 Coe, H., and Gallagher, M.: Measurements of dry deposition of NO₂ to a Dutch heathland
751 using the eddy-correlation technique, *Quarterly Journal of the Royal Meteorological Society*,
752 118, 767-786, 1992.

753 Cui, L., Li, R., Zhang, Y., Meng, Y., Fu, H., and Chen, J.: An observational study of nitrous
754 acid (HONO) in Shanghai, China: The aerosol impact on HONO formation during the haze
755 episodes, *Sci Total Environ*, 630, 1057-1070, 10.1016/j.scitotenv.2018.02.063, 2018.

756 Dillon, M. B.: Chemical evolution of the Sacramento urban plume: Transport and oxidation,
757 2002.

758 Ding, A., Nie, W., Huang, X., Chi, X., Sun, J., Kerminen, V.-M., Xu, Z., Guo, W., Petäjä, T.,
759 Yang, X., Kulmala, M., and Fu, C.: Long-term observation of air pollution-weather/climate
760 interactions at the SORPES station: a review and outlook, *Frontiers of Environmental Science
761 & Engineering*, 10, 10.1007/s11783-016-0877-3, 2016.

762 Ding, A. J., Fu, C. B., Yang, X. Q., Sun, J. N., Zheng, L. F., Xie, Y. N., Herrmann, E., Nie,
763 W., Petäjä, T., Kerminen, V. M., and Kulmala, M.: Ozone and fine particle in the western
764 Yangtze River Delta: an overview of 1 yr data at the SORPES station, *Atmospheric
765 Chemistry and Physics*, 13, 5813-5830, 10.5194/acp-13-5813-2013, 2013.

766 Dusanter, S., Vimal, D., Stevens, P., Volkamer, R., and Molina, L.: Measurements of OH and
767 HO₂ concentrations during the MCMA-2006 field campaign—Part 1: Deployment of the
768 Indiana University laser-induced fluorescence instrument, *Atmospheric Chemistry and
769 Physics*, 9, 1665-1685, 2009.

770 Elshorbany, Y. F., Kurtenbach, R., Wiesen, P., Lissi, E., Rubio, M., Villena, G., Gramsch, E.,
771 Rickard, A., Pilling, M., and Kleffmann, J.: Oxidation capacity of the city air of Santiago,
772 Chile, *Atmospheric Chemistry and Physics*, 9, 2257-2273, 2009.

773 Finlayson-Pitts, B. J., and Pitts, J. N.: CHAPTER 6 - Rates and Mechanisms of Gas-Phase
774 Reactions in Irradiated Organic – NO_x – Air Mixtures, in: *Chemistry of the Upper and Lower
775 Atmosphere*, edited by: Finlayson-Pitts, B. J., and Pitts, J. N., Academic Press, San Diego,
776 179-263, 2000.

777 Finlayson-Pitts, B. J., Wingen, L. M., Sumner, A. L., Syomin, D., and Ramazan, K. A.: The
778 heterogeneous hydrolysis of NO₂ in laboratory systems and in outdoor and indoor
779 atmospheres: An integrated mechanism, *Physical Chemistry Chemical Physics*, 5, 223-242,
780 10.1039/b208564j, 2003.

781 Fountoukis, C., and Nenes, A.: ISORROPIA II: a computationally efficient thermodynamic
782 equilibrium model for K⁺-Ca²⁺-Mg²⁺-NH₄⁽⁺⁾-Na⁺-SO₄²⁻-NO₃⁻-Cl⁻-H₂O aerosols,
783 *Atmospheric Chemistry and Physics*, 7, 4639-4659, 10.5194/acp-7-4639-2007, 2007.

784 George, C., Streckowski, R. S., Kleffmann, J., Stemmler, K., and Ammann, M.:
785 Photoenhanced uptake of gaseous NO₂ on solid organic compounds: a photochemical source
786 of HONO?, *Faraday Discussions*, 130, 195, 10.1039/b417888m, 2005.

787 Grassian, V.: Chemical reactions of nitrogen oxides on the surface of oxide, carbonate, soot,
788 and mineral dust particles: Implications for the chemical balance of the troposphere, *The*

789 Journal of Physical Chemistry A, 106, 860-877, 2002.

790 Han, C., Liu, Y., and He, H.: Heterogeneous reaction of NO₂ with soot at different relative
791 humidity, Environmental Science and Pollution Research, 24, 21248-21255,
792 10.1007/s11356-017-9766-y, 2017.

793 Hao, N., Zhou, B., Chen, D., and Chen, L.-m.: Observations of nitrous acid and its relative
794 humidity dependence in Shanghai, Journal of Environmental Sciences, 18, 910-915,
795 10.1016/s1001-0742(06)60013-2, 2006.

796 Harrison, R. M., Peak, J. D., and Collins, G. M.: Tropospheric cycle of nitrous acid, Journal
797 of Geophysical Research: Atmospheres, 101, 14429-14439, 1996.

798 Heland, J., Kleefmann, J., Kurtenbach, R., and Wiesen, P.: A new instrument to
799 measure gaseous nitrous acid (HONO) in the atmosphere, Environmental Science &
800 Technology, 35, 3207-3212, 2001.

801 Hendrick, F., Müller, J. F., Clémer, K., Wang, P., De Mazière, M., Fayt, C., Gielen, C.,
802 Hermans, C., Ma, J. Z., Pinardi, G., Stavrou, T., Vlemmix, T., and Van Roozendaal, M.:
803 Four years of ground-based MAX-DOAS observations of HONO and
804 NO₂ in the Beijing area, Atmospheric Chemistry and Physics, 14,
805 765-781, 10.5194/acp-14-765-2014, 2014.

806 Herrmann, H., Schaefer, T., Tilgner, A., Styler, S. A., Weller, C., Teich, M., and Otto, T.:
807 Tropospheric aqueous-phase chemistry: kinetics, mechanisms, and its coupling to a changing
808 gas phase, Chem Rev, 115, 4259-4334, 10.1021/cr500447k, 2015.

809 Hou, S., Tong, S., Ge, M., and An, J.: Comparison of atmospheric nitrous acid during severe
810 haze and clean periods in Beijing, China, Atmos. Environ., 124, 199-206,
811 10.1016/j.atmosenv.2015.06.023, 2016.

812 Huang, R. J., Yang, L., Cao, J., Wang, Q., Tie, X., Ho, K. F., Shen, Z., Zhang, R., Li, G., Zhu,
813 C., Zhang, N., Dai, W., Zhou, J., Liu, S., Chen, Y., Chen, J., and O'Dowd, C. D.:
814 Concentration and sources of atmospheric nitrous acid (HONO) at an urban site in Western
815 China, Sci Total Environ, 593-594, 165-172, 10.1016/j.scitotenv.2017.02.166, 2017.

816 Huang, X., Song, Y., Li, M., Li, J., Huo, Q., Cai, X., Zhu, T., Hu, M., and Zhang, H.: A
817 high-resolution ammonia emission inventory in China, Global Biogeochemical Cycles, 26,
818 n/a-n/a, 10.1029/2011gb004161, 2012.

819 Jarvis, D. L., Leaderer, B. P., Chinn, S., and Burney, P. G.: Indoor nitrous acid and
820 respiratory symptoms and lung function in adults, Thorax, 60, 474-479,
821 10.1136/thx.2004.032177, 2005.

822 Jenkin, M. E., Cox, R. A., and Williams, D. J.: Laboratory studies of the kinetics of formation
823 of nitrous acid from the thermal reaction of nitrogen dioxide and water vapour, Atmos.
824 Environ., 22, 487-498, 1988.

825 Kalberer, M., Ammann, M., Arens, F., Gäggeler, H. W., and Baltensperger, U.:
826 Heterogeneous formation of nitrous acid (HONO) on soot aerosol particles, Journal of
827 Geophysical Research: Atmospheres, 104, 13825-13832, 10.1029/1999jd900141, 1999.

828 Kanaya, Y., Cao, R., Akimoto, H., Fukuda, M., Komazaki, Y., Yokouchi, Y., Koike, M.,
829 Tanimoto, H., Takegawa, N., and Kondo, Y.: Urban photochemistry in central Tokyo: 1.
830 Observed and modeled OH and HO₂ radical concentrations during the winter and summer of
831 2004, Journal of Geophysical Research, 112, 10.1029/2007jd008670, 2007.

832 Khalizov, A. F., Cruz-Quinones, M., and Zhang, R.: Heterogeneous reaction of NO₂ on fresh

833 and coated soot surfaces, *The Journal of Physical Chemistry A*, 114, 7516-7524, 2010.

834 Kirchner, U., Scheer, V., and Vogt, R.: FTIR spectroscopic investigation of the mechanism
835 and kinetics of the heterogeneous reactions of NO₂ and HNO₃ with soot, *The Journal of*
836 *Physical Chemistry A*, 104, 8908-8915, 2000.

837 Kirchstetter, T., Harley, R., and Littlejohn, D.: Measurement of Nitrous Acid in Motor
838 Vehicle Exhaust, *Environmental Science & Technology Letters*, 30, 2843-2849,
839 10.1021/es960135y, 1996.

840 Kleffmann, J., Becker, K., and Wiesen, P.: Heterogeneous NO₂ conversion processes on acid
841 surfaces: Possible atmospheric implications, *Atmos. Environ.*, 32, 2721-2729,
842 10.1016/S1352-2310(98)00065-X, 1998.

843 Kleffmann, J., Becker, K. H., Lackhoff, M., and Wiesen, P.: Heterogeneous conversion of
844 NO₂ on carbonaceous surfaces, *Physical Chemistry Chemical Physics*, 1, 5443-5450, 1999.

845 Kleffmann, J.: Daytime formation of nitrous acid: A major source of OH radicals in a forest,
846 *Geophysical Research Letters*, 32, 10.1029/2005gl022524, 2005.

847 Kleffmann, J., Lörzer, J. C., Wiesen, P., Kern, C., Trick, S., Volkamer, R., Rodenas, M., and
848 Wirtz, K.: Intercomparison of the DOAS and LOPAP techniques for the detection of nitrous
849 acid (HONO), *Atmos. Environ.*, 40, 3640-3652, 10.1016/j.atmosenv.2006.03.027, 2006.

850 Kurtenbach, R., Becker, K., Gomes, J., Kleffmann, J., Lorzer, J., Spittler, M., Wiesen, P.,
851 Ackermann, R., Geyer, A., and Platt, U.: Investigations of emissions and heterogeneous
852 formation of HONO in a road traffic tunnel, *Atmos. Environ.*, 35, 3385-3394,
853 10.1016/S1352-2310(01)00138-8, 2001.

854 Lammel, G., and Cape, J. N.: Nitrous Acid and Nitrite in the Atmosphere, *CHEMICAL*
855 *SOCIETY REVIEWS*, 25, 361-369, 10.1039/cs9962500361, 1996.

856 Lammel, G.: Formation of nitrous acid: parameterisation and comparison with observations,
857 Max-Planck-Institut für Meteorologie, 1999.

858 Lee, J. D., Whalley, L. K., Heard, D. E., Stone, D., Dunmore, R. E., Hamilton, J. F., Young,
859 D. E., Allan, J. D., Laufs, S., and Kleffmann, J.: Detailed budget analysis of HONO in central
860 London reveals a missing daytime source, *Atmospheric Chemistry and Physics*, 16,
861 2747-2764, 10.5194/acp-16-2747-2016, 2016.

862 Li, D., Xue, L., Wen, L., Wang, X., Chen, T., Mellouki, A., Chen, J., and Wang, W.:
863 Characteristics and sources of nitrous acid in an urban atmosphere of northern China: Results
864 from 1-yr continuous observations, *Atmos. Environ.*, 182, 296-306,
865 10.1016/j.atmosenv.2018.03.033, 2018.

866 Li, X., Brauers, T., Häseler, R., Bohn, B., Fuchs, H., Hofzumahaus, A., Holland, F., Lou, S.,
867 Lu, K. D., Rohrer, F., Hu, M., Zeng, L. M., Zhang, Y. H., Garland, R. M., Su, H., Nowak, A.,
868 Wiedensohler, A., Takegawa, N., Shao, M., and Wahner, A.: Exploring the atmospheric
869 chemistry of nitrous acid (HONO) at a rural site in Southern China, *Atmospheric Chemistry*
870 *and Physics*, 12, 1497-1513, 10.5194/acp-12-1497-2012, 2012.

871 Lu, K. D., Rohrer, F., Holland, F., Fuchs, H., Bohn, B., Brauers, T., Chang, C. C., Haseler, R.,
872 Hu, M., Kita, K., Kondo, Y., Li, X., Lou, S. R., Nehr, S., Shao, M., Zeng, L. M., Wahner, A.,
873 Zhang, Y. H., and Hofzumahaus, A.: Observation and modelling of OH and HO₂
874 concentrations in the Pearl River Delta 2006: a missing OH source in a VOC rich atmosphere,
875 *Atmospheric Chemistry and Physics*, 12, 1541-1569, 10.5194/acp-12-1541-2012, 2012.

876 Lu, K. D., Hofzumahaus, A., Holland, F., Bohn, B., Brauers, T., Fuchs, H., Hu, M., Haseler,

877 R., Kita, K., Kondo, Y., Li, X., Lou, S. R., Oebel, A., Shao, M., Zeng, L. M., Wahner, A.,
878 Zhu, T., Zhang, Y. H., and Rohrer, F.: Missing OH source in a suburban environment near
879 Beijing: observed and modelled OH and HO₂ concentrations in summer 2006, *Atmospheric*
880 *Chemistry and Physics*, 13, 1057-1080, 10.5194/acp-13-1057-2013, 2013.

881 Meng, X.-L., Rosenthal, R., and Rubin, D. B.: Comparing correlated correlation coefficients,
882 *Psychological bulletin*, 111, 172, 1992.

883 Meng, Z., Lin, W., Jiang, X., Yan, P., Wang, Y., Zhang, Y., Jia, X., and Yu, X.:
884 Characteristics of atmospheric ammonia over Beijing, China, *Atmospheric Chemistry and*
885 *Physics*, 11, 6139-6151, 2011.

886 Meusel, H., Kuhn, U., Reiffs, A., Mallik, C., Harder, H., Martinez, M., Schuladen, J., Bohn,
887 B., Parchatka, U., Crowley, J. N., Fischer, H., Tomsche, L., Novelli, A., Hoffmann, T.,
888 Janssen, R. H. H., Hartogensis, O., Pikridas, M., Vrekoussis, M., Bourtsoukidis, E., Weber, B.,
889 Lelieveld, J., Williams, J., Pöschl, U., Cheng, Y., and Su, H.: Daytime formation of nitrous
890 acid at a coastal remote site in Cyprus indicating a common ground source of atmospheric
891 HONO and NO, *Atmospheric Chemistry and Physics*, 16, 14475-14493,
892 10.5194/acp-16-14475-2016, 2016.

893 Michoud, V., Colomb, A., Borbon, A., Miet, K., Beekmann, M., Camredon, M., Aumont, B.,
894 Perrier, S., Zapf, P., Siour, G., Ait-Helal, W., Afif, C., Kukui, A., Furger, M., Dupont, J. C.,
895 Haefelin, M., and Doussin, J. F.: Study of the unknown HONO daytime source at a European
896 suburban site during the MEGAPOLI summer and winter field campaigns, *Atmospheric*
897 *Chemistry and Physics*, 14, 2805-2822, 10.5194/acp-14-2805-2014, 2014.

898 Nie, W., Ding, A. J., Xie, Y. N., Xu, Z., Mao, H., Kerminen, V. M., Zheng, L. F., Qi, X. M.,
899 Huang, X., Yang, X. Q., Sun, J. N., Herrmann, E., Petäjä, T., Kulmala, M., and Fu, C. B.:
900 Influence of biomass burning plumes on HONO chemistry in eastern China, *Atmospheric*
901 *Chemistry and Physics*, 15, 1147-1159, 10.5194/acp-15-1147-2015, 2015.

902 Oswald, R., Behrendt, T., Ermel, M., Wu, D., Su, H., Cheng, Y., Breuninger, C., Moravek, A.,
903 Mougou, E., and Delon, C.: HONO emissions from soil bacteria as a major source of
904 atmospheric reactive nitrogen, *Science*, 341, 1233-1235, 2013.

905 Pagsberg, P., Bjergbakke, E., Ratajczak, E., and Sillesen, A.: Kinetics of the gas phase
906 reaction OH+ NO (+ M)→ HONO (+ M) and the determination of the UV absorption cross
907 sections of HONO, *Chemical physics letters*, 272, 383-390, 1997.

908 Perner, D., and Platt, U.: Detection of nitrous acid in the atmosphere by differential optical
909 absorption, *Geophysical Research Letters*, 6, 917-920, doi:10.1029/GL006i012p00917, 1979.

910 Platt, U., Perner, D., Harris, G. W., Winer, A. M., and Pitts, J. N.: Observations of nitrous
911 acid in an urban atmosphere by differential optical absorption, *Nature*, 285, 312-314,
912 10.1038/285312a0, 1980.

913 Qi, X. M., Ding, A. J., Nie, W., Petäjä, T., Kerminen, V. M., Herrmann, E., Xie, Y. N., Zheng,
914 L. F., Manninen, H., Aalto, P., Sun, J. N., Xu, Z. N., Chi, X. G., Huang, X., Boy, M.,
915 Virkkula, A., Yang, X. Q., Fu, C. B., and Kulmala, M.: Aerosol size distribution and new
916 particle formation in the western Yangtze River Delta of China: 2 years of measurements at
917 the SORPES station, *Atmospheric Chemistry and Physics*, 15, 12445-12464,
918 10.5194/acp-15-12445-2015, 2015.

919 Rappenglück, B., Lubertino, G., Alvarez, S., Golovko, J., Czader, B., and Ackermann, L.:
920 Radical precursors and related species from traffic as observed and modeled at an urban

921 highway junction, *Journal of the Air & Waste Management Association*, 63, 1270-1286,
922 10.1080/10962247.2013.822438, 2013.

923 Reisinger, A. R.: Observations of HNO₂ in the polluted winter atmosphere: possible
924 heterogeneous production on aerosols, *Atmos. Environ.*, 34, 3865-3874, 2000.

925 Richter, A., Burrows, J. P., Nuss, H., Granier, C., and Niemeier, U.: Increase in tropospheric
926 nitrogen dioxide over China observed from space, *Nature*, 437, 129-132,
927 10.1038/nature04092, 2005.

928 Rohde, R. A., and Muller, R. A.: Air Pollution in China: Mapping of Concentrations and
929 Sources, *PLoS One*, 10, e0135749, 10.1371/journal.pone.0135749, 2015.

930 Rohrer, F., and Berresheim, H.: Strong correlation between levels of tropospheric hydroxyl
931 radicals and solar ultraviolet radiation, *Nature*, 442, 184-187, 10.1038/nature04924, 2006.

932 Rohrer, F., Lu, K., Hofzumahaus, A., Bohn, B., Brauers, T., Chang, C.-C., Fuchs, H., Häseler,
933 R., Holland, F., Hu, M., Kita, K., Kondo, Y., Li, X., Lou, S., Oebel, A., Shao, M., Zeng, L.,
934 Zhu, T., Zhang, Y., and Wahner, A.: Maximum efficiency in the hydroxyl-radical-based
935 self-cleansing of the troposphere, *Nature Geoscience*, 7, 559-563, 10.1038/ngeo2199, 2014.

936 Saliba, N., Yang, H., and Finlayson-Pitts, B.: Reaction of gaseous nitric oxide with nitric acid
937 on silica surfaces in the presence of water at room temperature, *The Journal of Physical
938 Chemistry A*, 105, 10339-10346, 2001.

939 Seinfeld, J. H., and Pandis, S. N.: *Atmospheric chemistry and physics: from air pollution to
940 climate change*, John Wiley & Sons, 2016.

941 Shao, P., Xin, J., An, J., Kong, L., Wang, B., Wang, J., Wang, Y., and Wu, D.: The empirical
942 relationship between PM_{2.5} and AOD in Nanjing of the Yangtze River Delta, *Atmospheric
943 Pollution Research*, 8, 233-243, 10.1016/j.apr.2016.09.001, 2017.

944 Shen, Y., Virkkula, A., Ding, A., Wang, J., Chi, X., Nie, W., Qi, X., Huang, X., Liu, Q.,
945 Zheng, L., Xu, Z., Petäjä, T., Aalto, P. P., Fu, C., and Kulmala, M.: Aerosol optical properties
946 at SORPES in Nanjing, east China, *Atmospheric Chemistry and Physics*, 18, 5265-5292,
947 10.5194/acp-18-5265-2018, 2018.

948 Sleiman, M., Gundel, L. A., Pankow, J. F., Jacob, P., 3rd, Singer, B. C., and Destailhats, H.:
949 Formation of carcinogens indoors by surface-mediated reactions of nicotine with nitrous acid,
950 leading to potential thirdhand smoke hazards, *Proc Natl Acad Sci U S A*, 107, 6576-6581,
951 10.1073/pnas.0912820107, 2010.

952 Sörgel, M., Regelin, E., Bozem, H., Diesch, J. M., Drewnick, F., Fischer, H., Harder, H., Held,
953 A., Hosaynali-Beygi, Z., Martinez, M., and Zetzsch, C.: Quantification of the unknown
954 HONO daytime source and its relation to NO₂, *Atmospheric Chemistry and Physics*, 11,
955 10433-10447, 10.5194/acp-11-10433-2011, 2011.

956 Stemmler, K., Ammann, M., Donders, C., Kleffmann, J., and George, C.: Photosensitized
957 reduction of nitrogen dioxide on humic acid as a source of nitrous acid, *Nature*, 440, 195-198,
958 10.1038/nature04603, 2006.

959 Stemmler, K., Ndour, M., Elshorbany, Y., Kleffmann, J., D'anna, B., George, C., Bohn, B.,
960 and Ammann, M.: Light induced conversion of nitrogen dioxide into nitrous acid on
961 submicron humic acid aerosol, *Atmospheric Chemistry and Physics*, 7, 4237-4248, 2007.

962 Stutz, J., Kim, E. S., Platt, U., Bruno, P., Perrino, C., and Febo, A.: UV-visible absorption
963 cross sections of nitrous acid, *Journal of Geophysical Research: Atmospheres*, 105,
964 14585-14592, 10.1029/2000jd900003, 2000.

965 Stutz, J., Alicke, B., and Neftel, A.: Nitrous acid formation in the urban atmosphere: Gradient
966 measurements of NO₂ and HONO over grass in Milan, Italy, *Journal of Geophysical Research*,
967 107, 10.1029/2001jd000390, 2002.

968 Stutz, J., Alicke, B., Ackermann, R., Geyer, A., Wang, S., White, A. B., Williams, E. J.,
969 Spicer, C. W., and Fast, J. D.: Relative humidity dependence of HONO chemistry in urban
970 areas, *Journal of Geophysical Research: Atmospheres*, 109, n/a-n/a, 10.1029/2003jd004135,
971 2004.

972 Su, H., Cheng, Y. F., Cheng, P., Zhang, Y. H., Dong, S., Zeng, L. M., Wang, X., Slanina, J.,
973 Shao, M., and Wiedensohler, A.: Observation of nighttime nitrous acid (HONO) formation at
974 a non-urban site during PRIDE-PRD2004 in China, *Atmos. Environ.*, 42, 6219-6232,
975 10.1016/j.atmosenv.2008.04.006, 2008a.

976 Su, H., Cheng, Y. F., Shao, M., Gao, D. F., Yu, Z. Y., Zeng, L. M., Slanina, J., Zhang, Y. H.,
977 and Wiedensohler, A.: Nitrous acid (HONO) and its daytime sources at a rural site during the
978 2004 PRIDE-PRD experiment in China, *Journal of Geophysical Research*, 113,
979 10.1029/2007jd009060, 2008b.

980 Su, H., Cheng, Y., Oswald, R., Behrendt, T., Trebs, I., Meixner, F. X., Andreae, M. O., Cheng,
981 P., Zhang, Y., and Pöschl, U.: Soil nitrite as a source of atmospheric HONO and OH radicals,
982 *Science*, 333, 1616-1618, 2011.

983 Sumner, A. L., Menke, E. J., Dubowski, Y., Newberg, J. T., Penner, R. M., Hemminger, J. C.,
984 Wingen, L. M., Brauers, T., and Finlayson-Pitts, B. J.: The nature of water on surfaces of
985 laboratory systems and implications for heterogeneous chemistry in the troposphere, *Physical
986 Chemistry Chemical Physics*, 6, 10.1039/b308125g, 2004.

987 Sun, P., Nie, W., Chi, X., Xie, Y., Huang, X., Xu, Z., Qi, X., Xu, Z., Wang, L., Wang, T.,
988 Zhang, Q., and Ding, A.: Two years of online measurement of fine particulate nitrate in the
989 western Yangtze River Delta: influences of thermodynamics and
990 N_2O_5 hydrolysis, *Atmospheric Chemistry
991 and Physics*, 18, 17177-17190, 10.5194/acp-18-17177-2018, 2018.

992 Tan, Z., Fuchs, H., Lu, K., Hofzumahaus, A., Bohn, B., Broch, S., Dong, H., Gomm, S.,
993 Haeseler, R., He, L., Holland, F., Li, X., Liu, Y., Lu, S., Rohrer, F., Shao, M., Wang, B.,
994 Wang, M., Wu, Y., Zeng, L., Zhang, Y., Wahner, A., and Zhang, Y.: Radical chemistry at a
995 rural site (Wangdu) in the North China Plain: observation and model calculations of OH, HO₂
996 and RO₂ radicals, *Atmospheric Chemistry and Physics*, 17, 663-690,
997 10.5194/acp-17-663-2017, 2017.

998 Tan, Z., Rohrer, F., Lu, K., Ma, X., Bohn, B., Broch, S., Dong, H., Fuchs, H., Gkatzelis, G. I.,
999 Hofzumahaus, A., Holland, F., Li, X., Liu, Y., Liu, Y., Novelli, A., Shao, M., Wang, H., Wu,
1000 Y., Zeng, L., Hu, M., Kiendler-Scharr, A., Wahner, A., and Zhang, Y.: Wintertime
1001 photochemistry in Beijing: observations of RO_x radical concentrations in the North China
1002 Plain during the BEST-ONE campaign, *Atmospheric Chemistry and Physics*, 18,
1003 12391-12411, 10.5194/acp-18-12391-2018, 2018.

1004 Tong, S., Hou, S., Zhang, Y., Chu, B., Liu, Y., He, H., Zhao, P., and Ge, M.: Comparisons of
1005 measured nitrous acid (HONO) concentrations in a pollution period at urban and suburban
1006 Beijing, in autumn of 2014, *Science China Chemistry*, 58, 1393-1402,
1007 10.1007/s11426-015-5454-2, 2015.

1008 Underwood, G., Song, C., Phadnis, M., Carmichael, G., and Grassian, V.: Heterogeneous

1009 reactions of NO₂ and HNO₃ on oxides and mineral dust: A combined laboratory and
 1010 modeling study, *Journal of Geophysical Research: Atmospheres*, 106, 18055-18066, 2001.
 1011 VandenBoer, T., Markovic, M., Sanders, J., Ren, X., Pusede, S., Browne, E., Cohen, R.,
 1012 Zhang, L., Thomas, J., and Brune, W.: Evidence for a nitrous acid (HONO) reservoir at the
 1013 ground surface in Bakersfield, CA, during CalNex 2010, *Journal of Geophysical Research:*
 1014 *Atmospheres*, 119, 9093-9106, 2014a.
 1015 VandenBoer, T. C., Young, C. J., Talukdar, R. K., Markovic, M. Z., Brown, S. S., Roberts, J.
 1016 M., and Murphy, J. G.: Nocturnal loss and daytime source of nitrous acid through reactive
 1017 uptake and displacement, *Nature Geoscience*, 8, 55-60, 10.1038/ngeo2298, 2014b.
 1018 Villena, G., Kleffmann, J., Kurtenbach, R., Wiesen, P., Lissi, E., Rubio, M. A., Croxatto, G.,
 1019 and Rappenglück, B.: Vertical gradients of HONO, NO_x and O₃ in Santiago de Chile, *Atmos.*
 1020 *Environ.*, 45, 3867-3873, 10.1016/j.atmosenv.2011.01.073, 2011a.
 1021 Villena, G., Wiesen, P., Cantrell, C. A., Flocke, F., Fried, A., Hall, S. R., Hornbrook, R. S.,
 1022 Knapp, D., Kosciuch, E., Mauldin, R. L., McGrath, J. A., Montzka, D., Richter, D., Ullmann,
 1023 K., Walega, J., Weibring, P., Weinheimer, A., Staebler, R. M., Liao, J., Huey, L. G., and
 1024 Kleffmann, J.: Nitrous acid (HONO) during polar spring in Barrow, Alaska: A net source of
 1025 OH radicals?, *Journal of Geophysical Research*, 116, 10.1029/2011jd016643, 2011b.
 1026 Wang, G., Zhang, R., Gomez, M. E., Yang, L., Levy Zamora, M., Hu, M., Lin, Y., Peng, J.,
 1027 Guo, S., Meng, J., Li, J., Cheng, C., Hu, T., Ren, Y., Wang, Y., Gao, J., Cao, J., An, Z., Zhou,
 1028 W., Li, G., Wang, J., Tian, P., Marrero-Ortiz, W., Secret, J., Du, Z., Zheng, J., Shang, D.,
 1029 Zeng, L., Shao, M., Wang, W., Huang, Y., Wang, Y., Zhu, Y., Li, Y., Hu, J., Pan, B., Cai, L.,
 1030 Cheng, Y., Ji, Y., Zhang, F., Rosenfeld, D., Liss, P. S., Duce, R. A., Kolb, C. E., and Molina,
 1031 M. J.: Persistent sulfate formation from London Fog to Chinese haze, *Proc Natl Acad Sci U S*
 1032 *A*, 113, 13630-13635, 10.1073/pnas.1616540113, 2016.
 1033 Wang, J., Zhang, X., Guo, J., Wang, Z., and Zhang, M.: Observation of nitrous acid (HONO)
 1034 in Beijing, China: Seasonal variation, nocturnal formation and daytime budget, *Sci Total*
 1035 *Environ*, 587-588, 350-359, 10.1016/j.scitotenv.2017.02.159, 2017.
 1036 Wang, S.: Atmospheric observations of enhanced NO₂-HONO conversion on mineral dust
 1037 particles, *Geophysical Research Letters*, 30, 10.1029/2003gl017014, 2003.
 1038 Wang, S., Zhou, R., Zhao, H., Wang, Z., Chen, L., and Zhou, B.: Long-term observation of
 1039 atmospheric nitrous acid (HONO) and its implication to local NO₂ levels in Shanghai, China,
 1040 *Atmos. Environ.*, 77, 718-724, 10.1016/j.atmosenv.2013.05.071, 2013.
 1041 Wentzell, J. J. B., Schiller, C. L., and Harris, G. W.: Measurements of HONO during
 1042 BAQS-Met, *Atmospheric Chemistry and Physics*, 10, 12285-12293,
 1043 10.5194/acp-10-12285-2010, 2010.
 1044 Wong, K. W., Oh, H. J., Lefer, B. L., Rappenglück, B., and Stutz, J.: Vertical profiles of
 1045 nitrous acid in the nocturnal urban atmosphere of Houston, TX, *Atmospheric Chemistry and*
 1046 *Physics*, 11, 3595-3609, 10.5194/acp-11-3595-2011, 2011.
 1047 Xie, Y., Ding, A., Nie, W., Mao, H., Qi, X., Huang, X., Xu, Z., Kerminen, V.-M., Petäjä, T.,
 1048 Chi, X., Virkkula, A., Boy, M., Xue, L., Guo, J., Sun, J., Yang, X., Kulmala, M., and Fu, C.:
 1049 Enhanced sulfate formation by nitrogen dioxide: Implications from in situ observations at the
 1050 SORPES station, *Journal of Geophysical Research: Atmospheres*, 120, 12679-12694,
 1051 10.1002/2015jd023607, 2015.
 1052 Xu, Z., Wang, T., Xue, L. K., Louie, P. K. K., Luk, C. W. Y., Gao, J., Wang, S. L., Chai, F.

1053 H., and Wang, W. X.: Evaluating the uncertainties of thermal catalytic conversion in
1054 measuring atmospheric nitrogen dioxide at four differently polluted sites in China, *Atmos.*
1055 *Environ.*, 76, 221-226, 10.1016/j.atmosenv.2012.09.043, 2013.

1056 Xu, Z., Wang, T., Wu, J., Xue, L., Chan, J., Zha, Q., Zhou, S., Louie, P. K. K., and Luk, C. W.
1057 Y.: Nitrous acid (HONO) in a polluted subtropical atmosphere: Seasonal variability, direct
1058 vehicle emissions and heterogeneous production at ground surface, *Atmos. Environ.*, 106,
1059 100-109, 10.1016/j.atmosenv.2015.01.061, 2015.

1060 Xu, Z., Huang, X., Nie, W., Chi, X., Xu, Z., Zheng, L., Sun, P., and Ding, A.: Influence of
1061 synoptic condition and holiday effects on VOCs and ozone production in the Yangtze River
1062 Delta region, China, *Atmos. Environ.*, 168, 112-124, 10.1016/j.atmosenv.2017.08.035, 2017.

1063 Xu, Z., Huang, X., Nie, W., Shen, Y., Zheng, L., Xie, Y., Wang, T., Ding, K., Liu, L., Zhou,
1064 D., Qi, X., and Ding, A.: Impact of Biomass Burning and Vertical Mixing of Residual-Layer
1065 Aged Plumes on Ozone in the Yangtze River Delta, China: A Tethered-Balloon Measurement
1066 and Modeling Study of a Multiday Ozone Episode, *Journal of Geophysical Research:*
1067 *Atmospheres*, 123, 11,786-711,803, 10.1029/2018jd028994, 2018.

1068 Yabushita, A., Enami, S., Sakamoto, Y., Kawasaki, M., Hoffmann, M. R., and Colussi, A. J.:
1069 Anion-Catalyzed Dissolution of NO₂ on Aqueous Microdroplets, *J. Phys. Chem. A*, 113,
1070 4844-4848, 10.1021/jp900685f, 2009.

1071 Ye, C., Zhou, X., Pu, D., Stutz, J., Festa, J., Spolaor, M., Tsai, C., Cantrell, C., Mauldin, R. L.,
1072 3rd, Campos, T., Weinheimer, A., Hornbrook, R. S., Apel, E. C., Guenther, A., Kaser, L.,
1073 Yuan, B., Karl, T., Haggerty, J., Hall, S., Ullmann, K., Smith, J. N., Ortega, J., and Knote, C.:
1074 Rapid cycling of reactive nitrogen in the marine boundary layer, *Nature*, 532, 489-491,
1075 10.1038/nature17195, 2016.

1076 Ye, C., Zhang, N., Gao, H., and Zhou, X.: Photolysis of Particulate Nitrate as a Source of
1077 HONO and NO_x, *Environ Sci Technol*, 51, 6849-6856, 10.1021/acs.est.7b00387, 2017.

1078 Yu, Y., Galle, B., Panday, A., Hodson, E., Prinn, R., and Wang, S.: Observations of high rates
1079 of NO₂-HONO conversion in the nocturnal atmospheric boundary layer in Kathmandu, Nepal,
1080 *ATMOSPHERIC CHEMISTRY AND PHYSICS*, 9, 6401-6415, 10.5194/acp-9-6401-2009,
1081 2009.

1082 Zhou, L., Wang, W., Hou, S., Tong, S., and Ge, M.: Heterogeneous uptake of nitrogen
1083 dioxide on Chinese mineral dust, *J Environ Sci (China)*, 38, 110-118,
1084 10.1016/j.jes.2015.05.017, 2015.

1085 Zhou, X., Civerolo, K., Dai, H., Huang, G., Schwab, J., and Demerjian, K.: Summertime
1086 nitrous acid chemistry in the atmospheric boundary layer at a rural site in New York State,
1087 *Journal of Geophysical Research: Atmospheres*, 107, ACH 13-11-ACH 13-11,
1088 10.1029/2001jd001539, 2002.

1089 Zhou, X., Gao, H., He, Y., Huang, G., Bertman, S. B., Civerolo, K., and Schwab, J.: Nitric
1090 acid photolysis on surfaces in low-NO_x environments: Significant atmospheric implications,
1091 *Geophysical Research Letters*, 30, n/a-n/a, 10.1029/2003gl018620, 2003.

1092 Zhou, X., Zhang, N., TerAvest, M., Tang, D., Hou, J., Bertman, S., Alaghmand, M., Shepson,
1093 P. B., Carroll, M. A., Griffith, S., Dusanter, S., and Stevens, P. S.: Nitric acid photolysis on
1094 forest canopy surface as a source for tropospheric nitrous acid, *Nature Geoscience*, 4, 440-443,
1095 10.1038/ngeo1164, 2011.

1096

Tables

Table 1. Sources and sinks for nitrous acid (HONO) in the troposphere.

Budget	Occurrence	Pathways	Abbr.
Sinks	Only daytime	$\text{HONO} + h\nu \xrightarrow{320-400\text{nm}} \text{OH} + \text{NO}$	R1
	Mainly daytime	$\text{HONO} + \text{OH} \rightarrow \text{NO}_2 + \text{H}_2\text{O}$	R2
	All day	Deposition/heterogeneous loss on aerosol	/
Sources	Mainly daytime	$\text{NO} + \text{OH} \xrightarrow{\text{M}} \text{HONO}$	R3
	Mainly nighttime	$2\text{NO}_{2(\text{g})} + \text{H}_2\text{O}_{(\text{ads})} \xrightarrow{\text{surf}} \text{HONO}_{(\text{g})} + \text{HNO}_{3(\text{ads})}$	R4
	Mainly daytime	$\text{NO}_{2(\text{g})} + \text{HC}_{\text{red}} \xrightarrow{\text{surf}} \text{HONO}_{(\text{g})} + \text{HC}_{\text{ox}}$	R5
	Only daytime	$\text{HNO}_3 / \text{NO}_3^- + h\nu \xrightarrow{\text{surf}} \text{HONO} / \text{NO}_2^- + \text{O}$	R6
	All day	Release of soil nitrite	/
	All day	Combustion emission(fossil and biomass)	/

Table 2. Overview of the measured HONO and NO_x levels in Nanjing and comparison with other urban or suburban sites.

Location	Date	HONO(ppb)		NO ₂ (ppb)		NO _x (ppb)		HONO/NO ₂		HONO/NO _x		Ref
		Night	Day	Night	Day	Night	Day	Night	Day	Night	Day	
Rome(Italy)	May-Jun 2001	1.00	0.15	27.2	4.0	51.2	4.2	0.037	0.038	0.020	0.036	1
Kathmandu(Nepal)	Jan-Feb 2003	1.74	0.35	17.9	8.6	20.1	13.0	0.097	0.041	0.087	0.027	2
Tokto(Japan)	Jan-Feb 2004	0.80	0.05	31.8	18.2	37.4	26.3	0.025	0.003	0.021	0.002	3
Santiago(Chile)	Mar 2005	3.00	1.50	30.0	20.0	200.0	40.0	0.100	0.075	0.015	0.038	4
Mexico City(Mexico)	Mar 2006	/	0.43	/	28.4	/	44.8	/	0.015	/	0.010	5
Houston(USA)	Sep 2006	0.50	0.10	20.0	10.0	/	/	0.025	0.010	/	/	6
Shanghai(China)	Oct 2009	1.50	1.00	41.9	30.0	/	/	0.038	0.032	/	/	7
Hongkong(China)	Aug 2011	0.66	0.70	21.8	18.1	29.3	29.3	0.031	0.042	0.025	0.028	8
	Nov 2011	0.95	0.89	27.2	29.0	37.2	40.6	0.034	0.030	0.028	0.021	
	Feb 2012	0.88	0.92	22.2	25.8	37.8	48.3	0.036	0.035	0.025	0.020	
	May 2012	0.33	0.40	14.7	15.0	19.1	21.1	0.022	0.030	0.019	0.022	
Beijing(China)	Oct–Nov 2014	1.75	0.93	37.6	35.3	94.5	53.4	0.047	0.026	0.019	0.017	9
Xi'an(China)	Jul–Aug 2015	0.51	1.57	15.4	24.7	/	/	0.033	0.062	/	/	10
Jinan(China)	Sep–Nov 2015	0.87	0.66	25.4	23.2	38.0	37.5	0.049	0.034	0.034	0.022	11
	Dec 2015-Feb 2016	2.15	1.35	41.1	34.6	78.5	64.8	0.056	0.047	0.034	0.031	
	Mar–May 2016	1.24	1.04	35.8	25.8	47.3	36.0	0.046	0.052	0.035	0.041	
	Jun–Aug 2016	1.20	1.01	22.5	19.0	29.1	25.8	0.106	0.079	0.060	0.049	
Nanjing(China)	Nov 2017-Nov 2018	0.80	0.57	18.9	13.9	24.9	19.3	0.045	0.044	0.041	0.036	this study
	Dec-Feb(winter)	1.15	0.92	28.4	23.1	45.5	37.7	0.040	0.038	0.029	0.025	
	Mar–May(spring)	0.76	0.59	17.4	12.9	19.1	15.9	0.048	0.049	0.046	0.042	
	Jun–Aug(summer)	0.56	0.34	12.5	7.7	13.5	9.1	0.048	0.051	0.046	0.045	
	Sep–Nov(autumn)	0.81	0.51	18.9	13.4	25.1	17.7	0.044	0.035	0.039	0.029	

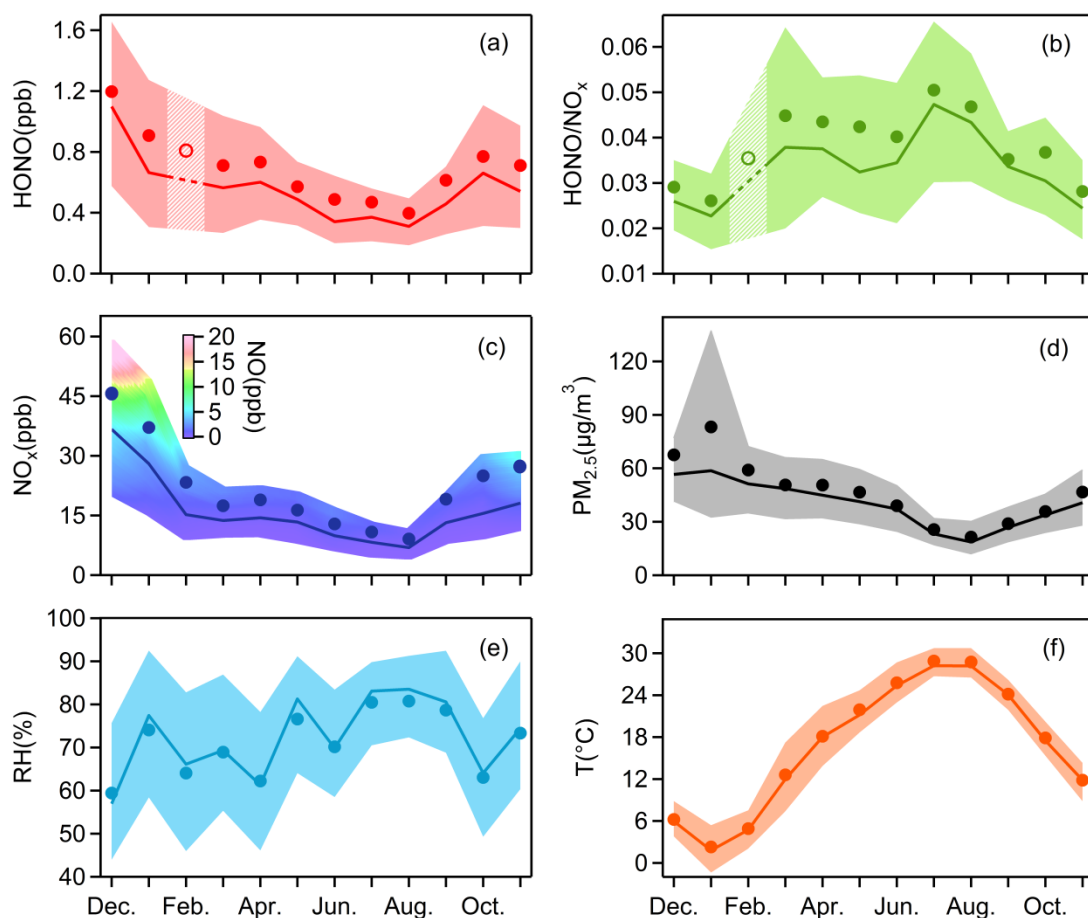
1: Acker et al. (2006); 2: Yu et al. (2009); 3: Kanaya et al. (2007); 4: Elshorbany et al. (2009); 5: Dusanter et al. (2009); 6: Wong et al. (2011); 7: Bernard et al. (2016); 8: Xu et al. (2015); 9: Tong et al. (2015); 10: Huang et al. (2017); 11: Li et al. (2018)

Table 3. Correlations of P_{unknown} against various parameters.

Parameters	Winter		Spring		Summer		Autumn	
	r	N	r	N	r	N	r	N
NO ₂	0.46	220	0.33	280	0.07	366	0.15	348
PM _{2.5}	0.41	220	0.43	280	0.22	366	0.26	348
NO ₃ ⁻	0.39	211	0.41	270	-0.01	353	0.19	344
SO ₄ ²⁻	0.34	204	0.26	270	0.15	357	0.23	337
NH ₄ ⁺	0.38	211	0.36	273	0.09	360	0.22	332
RH	0.00	220	-0.33	280	-0.37	366	-0.19	348
UVB	0.22	220	0.44	280	0.43	366	0.45	348
NO ₂ *PM _{2.5}	0.42	220	0.43	280	0.10	366	0.23	348
NO ₂ *NO ₃ ⁻	0.40	211	0.43	270	-0.04	353	0.20	344
NO ₂ *SO ₄ ²⁻	0.41	204	0.35	270	0.08	357	0.22	337
NO ₂ *NH ₄ ⁺	0.41	211	0.41	273	0.05	360	0.21	332
UVB*NO ₂	0.59	220	0.68	280	0.49	366	0.65	348
UVB*PM _{2.5}	0.53	220	0.64	280	0.51	366	0.65	348
UVB*NO ₃ ⁻	0.50	211	0.56	270	0.25	353	0.46	344
UVB*SO ₄ ²⁻	0.42	204	0.49	270	0.42	357	0.55	337
UVB*NH ₄ ⁺	0.47	211	0.53	273	0.35	360	0.52	332
NO ₂ *UVB*PM _{2.5}	0.53	220	0.64	280	0.39	366	0.55	348

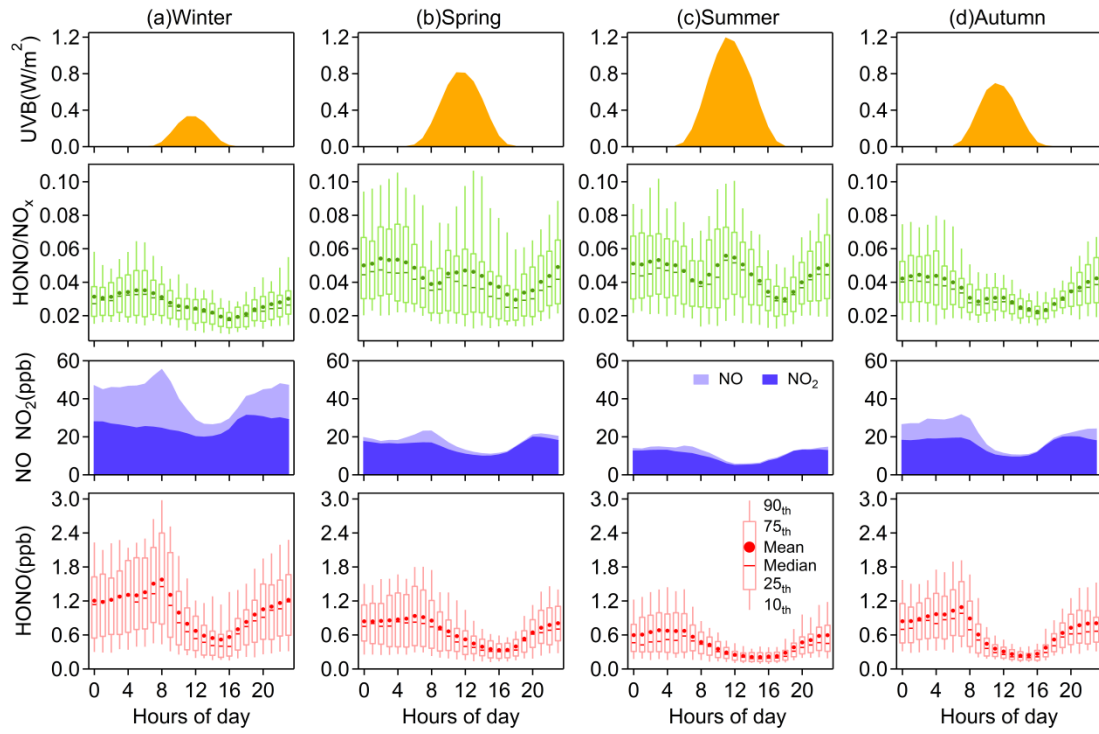
1097 **Figures**

1098



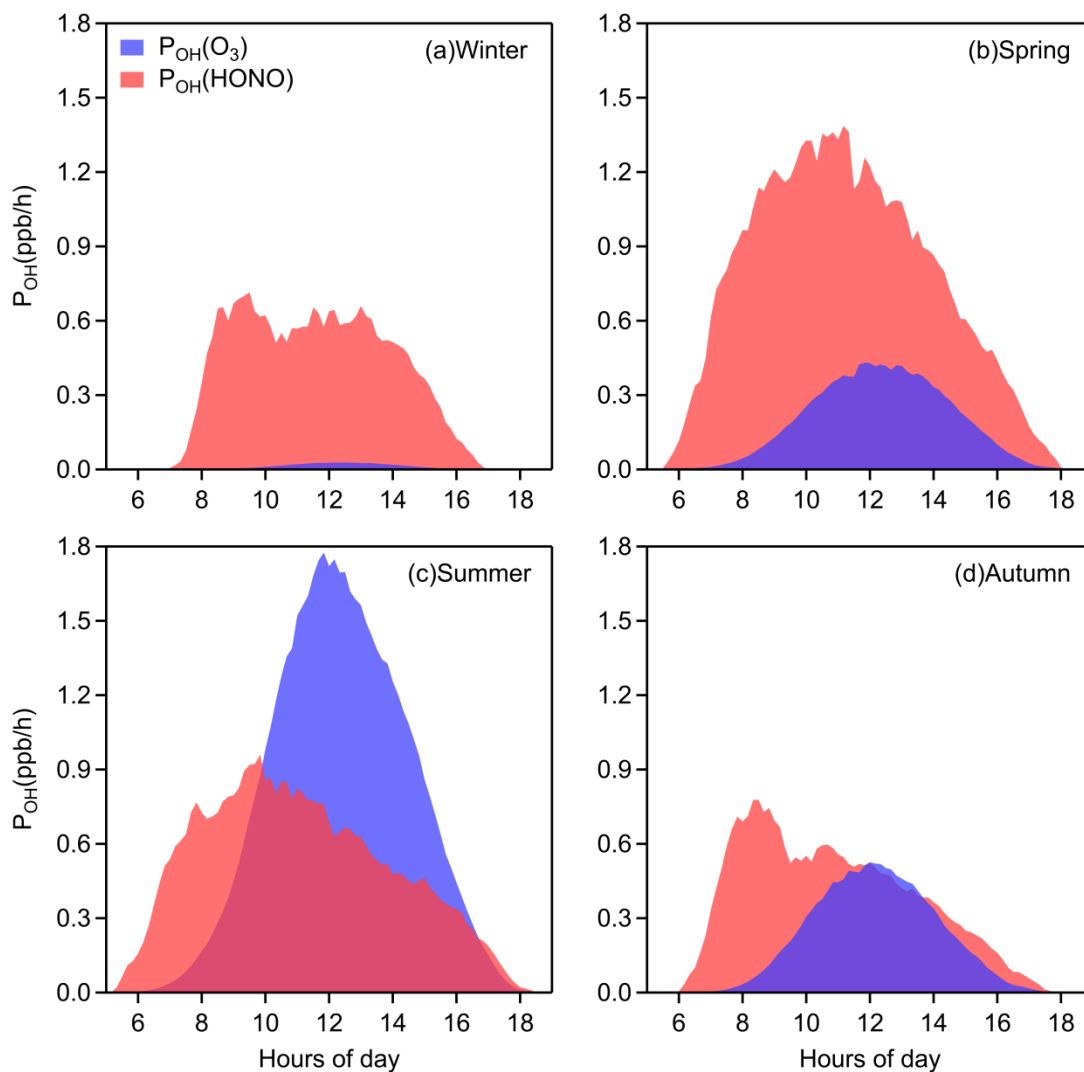
1099

1100 **Fig. 1.** Monthly variations of (a) HONO, (b) HONO/NO_x, (c) NO_x, (d) PM_{2.5}, (e) RH and (f) T.
 1101 The solid bold lines are median values, the markers indicate mean values, and the shaded areas
 1102 represent percentiles of 75% and 25%. In (a) and (b), values in February are linearly interpolated
 1103 based on the data from the months before and after, since there were only few days when HONO
 1104 was observed in February. In (c), the shaded area is colored by the 25th to the 75th percentiles of
 1105 NO.
 1106



1107
 1108
 1109
 1110

Fig. 2. Diurnal variations of HONO, NO, NO₂, HONO/NO_x, UVB in (a) winter, (b) spring, (c) summer, (d) autumn. The levels of NO, NO₂ and UVB are displayed as their mean concentrations.



1111

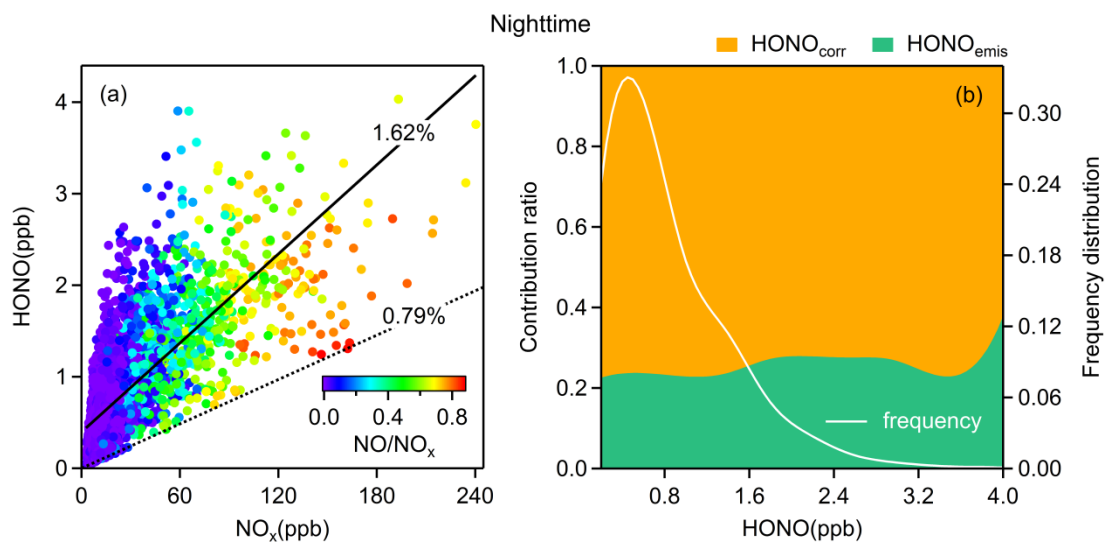
1112 **Fig. 3.** Averaged OH production rates from photolysis of HONO and ozone in (a) winter, (b)
 1113 spring, (c) summer, and (d) autumn. The $P_{OH}(HONO)$ here is actually the net OH production rate,
 1114 by subtracting the consumption of OH radicals by R2 and R3. The mean values of $P_{OH}(HONO)$ at
 1115 daytime (08:00-16:00 LT) are: 0.53 ppb/h in winter, 1.02 ppb/h in spring, 0.66 ppb/h in summer,
 1116 0.47 ppb/h in autumn.

1117

1118

1119

1120



1121

1122 **Fig. 4.** (a) The relationship between HONO and NO_x colored by the NO/NO_x ratio. The dotted line
 1123 is the emission ratio derived in this study and the solid line is obtained from simple linear fitting;
 1124 (b) average emission contribution ratios for different concentrations of HONO and the frequency
 1125 distribution of HONO concentrations. Both (a) and (b) are nighttime values.

1126

1127

1128

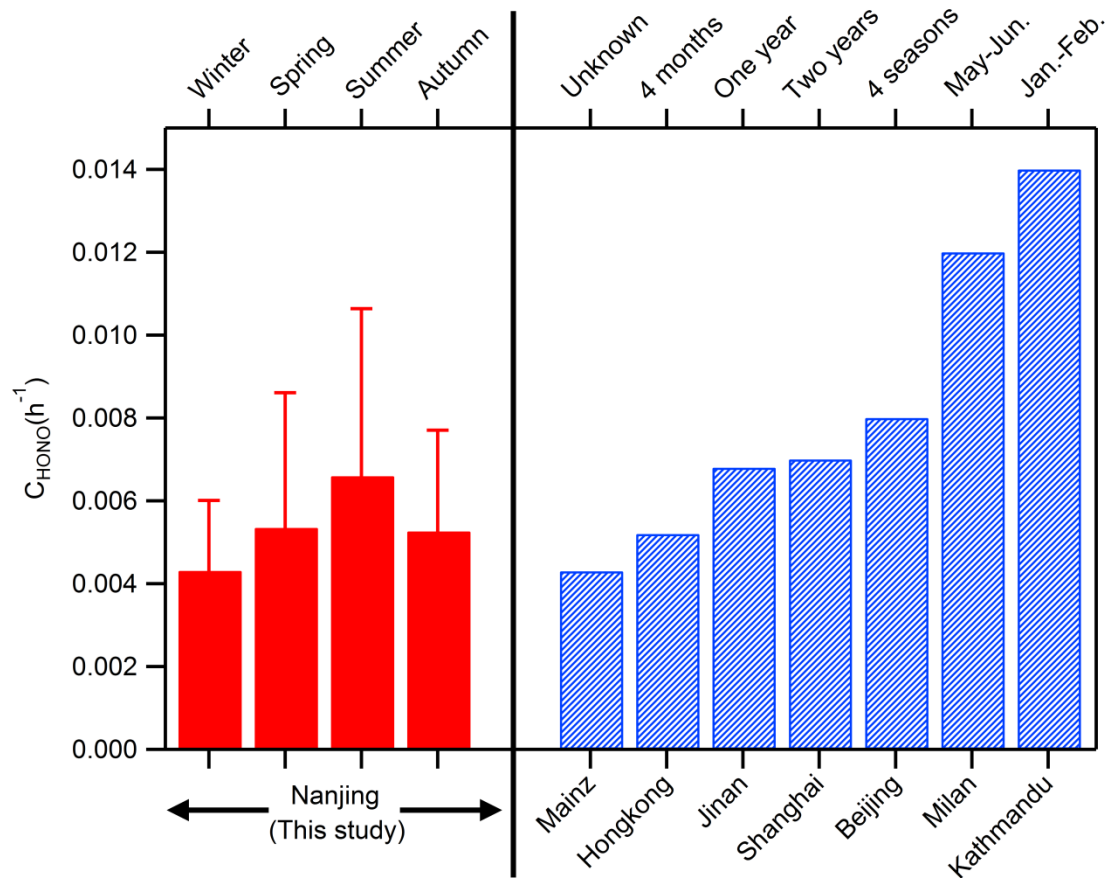
1129

1130

1131

1132

1133



1134

Fig. 5. Comparison of observed NO₂ to HONO conversion rates in cities: Nanjing (this study); Mainz (Lammel, 1999); Hongkong (Xu et al., 2015); Jinan (Li et al., 2018); Shanghai (Wang et al., 2013); Beijing (Wang et al., 2017); Milan (Alicke et al., 2002); and Kathmandu (Yu et al., 2009).

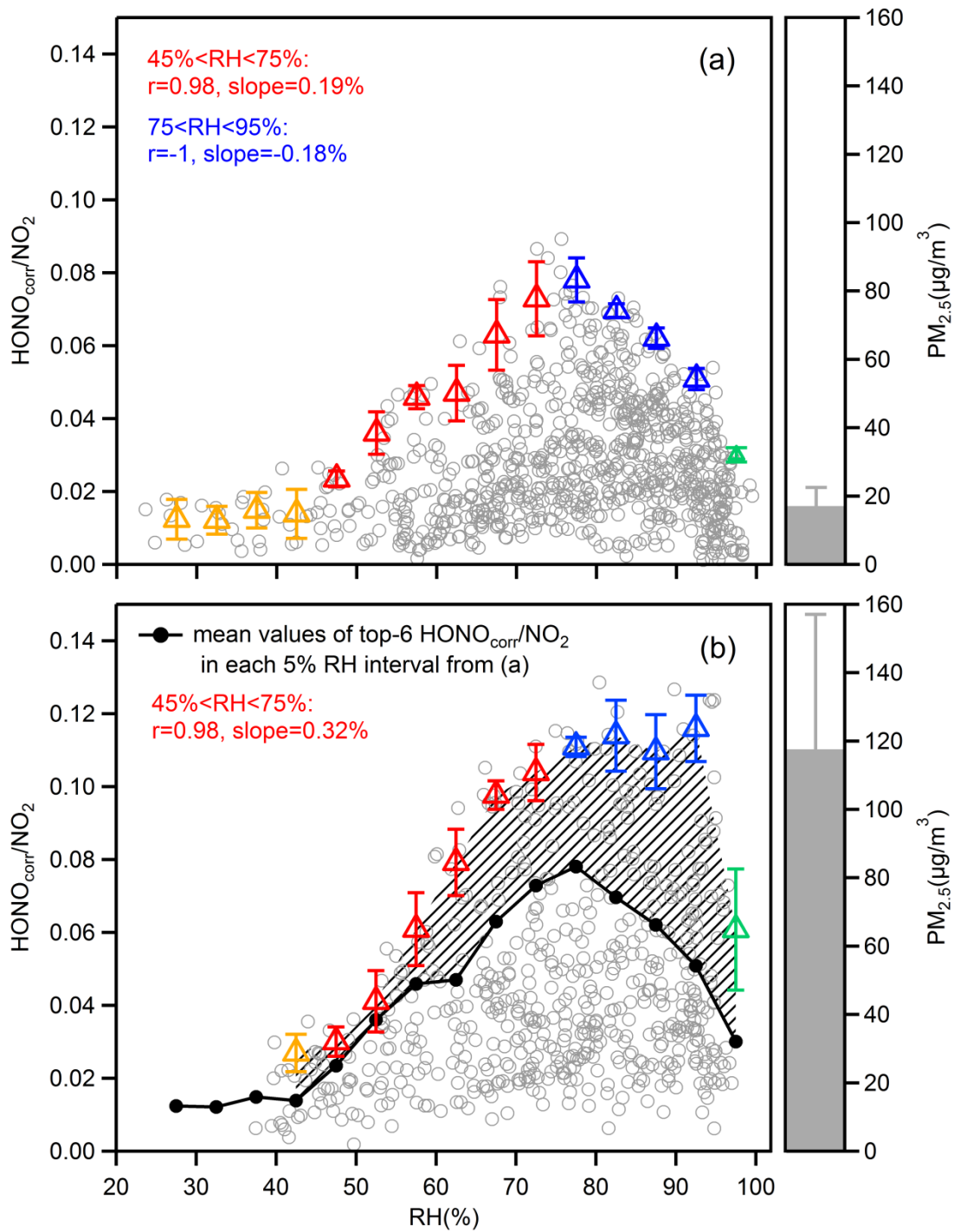


Fig. 6. Scatter plot of the HONO_{corr}/NO₂ ratio and RH during nighttime, separating the data into (a) clean hours (hourly mean PM_{2.5} < 25 µg/m³) and (b) polluted hours (hourly mean PM_{2.5} > 75 µg/m³). Triangles are the averaged top-6 HONO_{corr}/NO₂ in each 5% RH interval, and the error bars are the standard deviations. The overall average concentrations of PM_{2.5} in (a) and (b) are shown to the right of the figures.

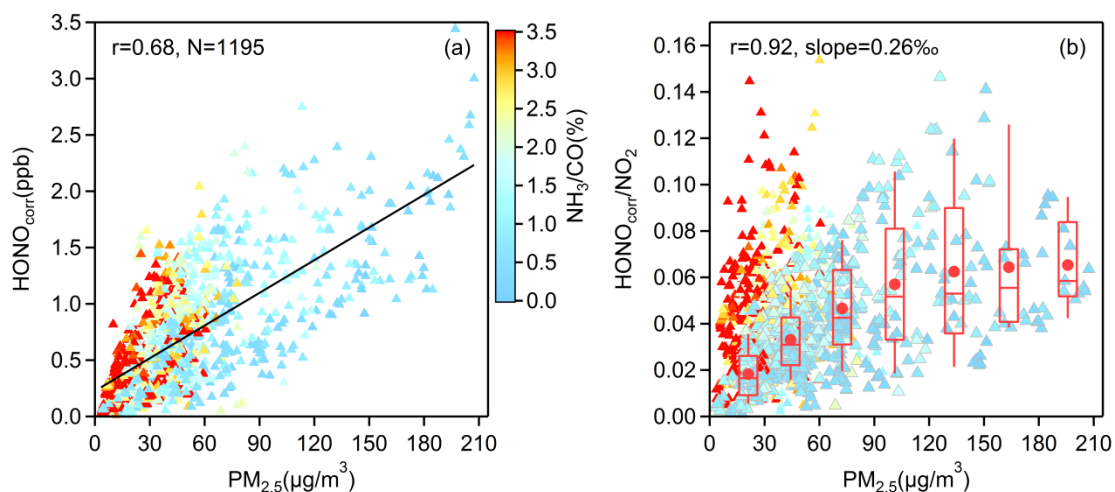


Fig. 7. (a) The correlation between $\text{HONO}_{\text{corr}}$ and $\text{PM}_{2.5}$, and (b) the correlation between $\text{HONO}_{\text{corr}}/\text{NO}_2$ and $\text{PM}_{2.5}$, all scatters come from the time (3:00-6:00 LT) when the $\text{HONO}_{\text{corr}}/\text{NO}_2$ ratio reaches the pseudo steady state at each night and are colored by NH_3/CO . In (b), the larger triangles with gray borders, depict the measured data from November to May, and the boxplot in each $30 \mu\text{g}/\text{m}^3$ interval of $\text{PM}_{2.5}$ is illustrated according to the same data, the red box boundaries represent interquartile range, the whiskers represent the 10%–90% percentile range, the horizontal red lines represent median values and the red markers represent mean values. The correlation coefficient and the slope of the linearly fitted line in (b) are derived from the averaged $\text{HONO}_{\text{corr}}/\text{NO}_2$ and averaged $\text{PM}_{2.5}$ in each box.

1135

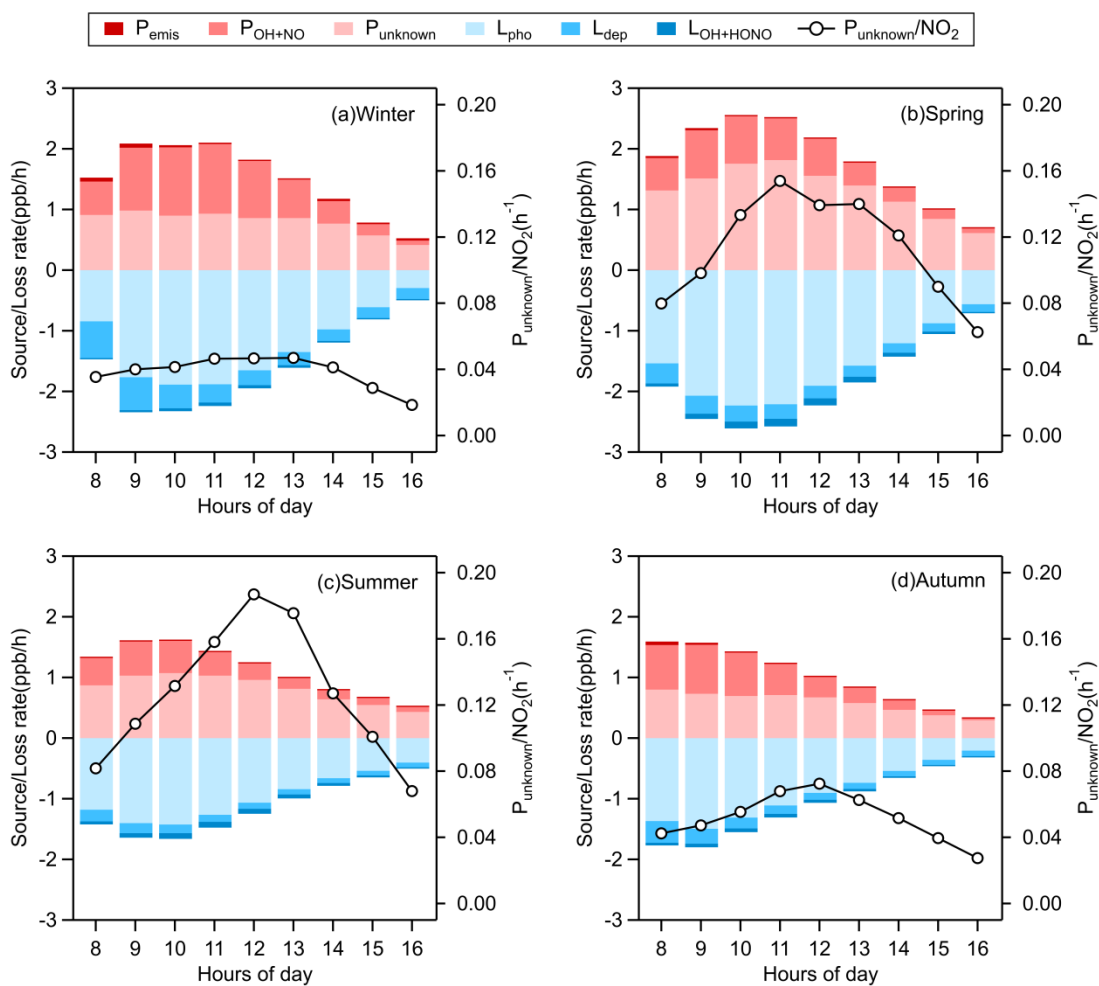


Fig. 8. Averaged daytime HONO budget and the missing source strength (P_{unknown}) normalized by NO_2 in (a) winter, (b) spring, (c) summer, and (d) autumn. The mean values of P_{unknown} around noontime (10:00-14:00 LT) are: 0.91 ppb/h in winter, 1.61 ppb/h in Spring, 0.98 ppb/h in summer, 0.68 ppb/h in autumn.

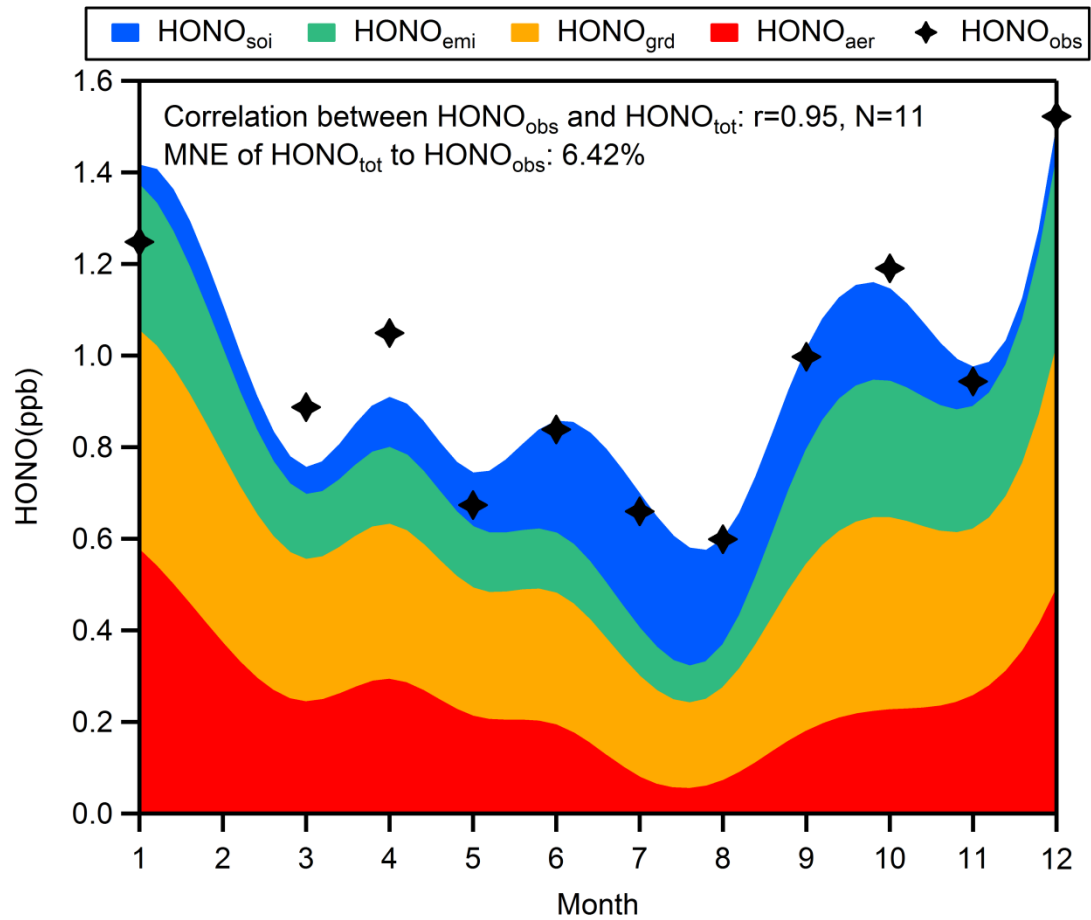


Fig. 9. Seasonal variations of 4 sources of HONO at night (3:00-6:00 LT). The mean normalized error (MNE) of HONO_{tot} to HONO_{obs} is 6.42%.